

# **US-APWR CONTAINMENT PERFORMANCE FOR PRESSURE LOADS**

**Non-Proprietary Version**

**June 2010**

**©2010 Mitsubishi Heavy Industries, Ltd.  
All Rights Reserved**

**Revision History**

Revision	Page	Description
0	All	Original Issue

**© 2010**  
**MITSUBISHI HEAVY INDUSTRIES, LTD.**  
**All Rights Reserved**

This document has been prepared by Mitsubishi Heavy Industries, Ltd. ("MHI") in connection with the U.S. Nuclear Regulatory Commission's ("NRC") licensing review of MHI's US-APWR nuclear power plant design. No right to disclose, use or copy any of the information in this document, other than that by the NRC and its contractors in support of the licensing review of the US-APWR, is authorized without the express written permission of MHI.

This document contains technology information and intellectual property relating to the US-APWR and it is delivered to the NRC on the express condition that it not be disclosed, copied or reproduced in whole or in part, or used for the benefit of anyone other than MHI without the express written permission of MHI, except as set forth in the previous paragraph.

This document is protected by the laws of Japan, U.S. copyright law, international treaties and conventions, and the applicable laws of any country where it is being used.

Mitsubishi Heavy Industries, Ltd.  
16-5, Konan 2-chome, Minato-ku  
Tokyo 108-8215 Japan

## **Abstract**

The purpose of this technical report is to present the Containment Performance for Pressure Loads. The analyses described herein are provided to establish the fragility of the US-APWR primary containment system for over-pressurization. The fragility is calculated for 3 specified thermal conditions, namely, steady state normal operating temperatures, steady state conditions representing long term accident conditions, and transient thermal conditions for a representative hydrogen burning condition involving much higher temperatures but for much shorter durations.

## Table of Contents

<b>List of Tables</b>	<b>ii</b>
<b>List of Figures</b>	<b>iii</b>
<b>List of Acronyms</b>	<b>v</b>
<b>1.0 SCOPE</b>	<b>1</b>
<b>2.0 SUMMARY DESCRIPTION</b>	<b>2</b>
<b>3.0 ANALYSIS METHODS</b>	<b>5</b>
3.1 Finite Element Modeling	5
3.2 Loading Conditions	6
3.3 Probabilistic Assessment	7
3.4 Uncertainty in Parameter Variability	8
3.5 Uncertainty in Modeling and Processes	10
3.6 Thermal Conditions	12
3.7 Material Properties	17
3.8 Concrete Performance	22
3.9 Failure Criteria	26
<b>4.0 PRESTRESSED CONCRETE CONTAINMENT</b>	<b>28</b>
4.1 Model Description	28
4.2 Thermal Analyses	33
4.3 Median Capacity Analyses	37
4.4 Evaluation for Uncertainty	47
4.5 Fragility Summary	48
<b>5.0 APPLICABLE DOCUMENTS</b>	<b>52</b>
5.1 Project Documents	52
5.2 Codes and Standards	52
5.3 Reference Documents	52

## List of Tables

<u>Table No.</u>	<u>Title</u>	<u>Page</u>
2-1	Summary of US-APWR Fragility for Over-Pressurization	3
3-1	Summary of Variance for Modeling Uncertainty	11
3-2	Summary of Temperature Conditions	13
3-3	Temperature and Pressure in PCCV for Long Term Accident Thermal Condition	13
3-4	Temperature and Pressure in PCCV for Hydrogen Burning Thermal Condition	14
3-5	Film Coefficients for Thermal Conditions	14
3-6	Summary of Thermal Material Properties	18
3-7	Summary of Elastic Mechanical Properties for Steels	19
3-8	Summary of Plastic Mechanical Properties for Steels	19
3-9	Summary of Concrete Material Properties	20
3-10	Summary of Material Limits and Failure Criteria	27
4-1	Summary of Median Pressure Capacities	37
4-2	Summary of Uncertainty Evaluations in Global Modeling	47
4-3	Summary of Pressure Fragility from Global Modeling	49

## List of Figures

<u>Figure No.</u>	<u>Title</u>	<u>Page</u>
2-1	Pressure Fragility under Normal Operating Thermal Conditions (105 °F)	3
2-2	Pressure Fragility under Long Term Accident Thermal Conditions (438 °F)	4
2-3	Pressure Fragility under Hydrogen Burning Thermal Conditions (1000 °F)	4
3-1	Calculation of Variance due to Modeling Uncertainty	11
3-2	Thermal Conditions on Exterior Surfaces of PCCV	15
3-3	Temperature and Pressure for Long Term Accident Condition	16
3-4	Temperature and Pressure for Hydrogen Burning Condition	16
3-5	Illustration of Stress-Strain Relations for A615 Grade 60 Rebar	21
3-6	Illustration of Stress-Strain Relations for A5-6 Grade 60 Liner Plate	22
3-7	Crack Initiation Criteria Curve	23
3-8	Shear Modulus Reduction for Open Cracks	24
3-9	Example of Shear Stress Capacity Across Open Cracks	24
3-10	Uniaxial Compressive Strength as Function of Temperature	25
4-1	Full 3D Finite Element Modeling for Thermal Analysis	29
4-2	Full 3D Finite Element Modeling for Stress Analysis	30
4-3	Illustration of Modeling for Tendons	30
4-4	Modeling of Reinforcement, Inside Axial Bars	31
4-5	Modeling of Reinforcement, Outside Axial Bars	31
4-6	Modeling of Reinforcement, Inside Hoop Bars	32
4-7	Modeling of Reinforcement, Outside Hoop Bars	32
4-8	Modeling of Reinforcement, Other Bars	33
4-9	Temperature Distribution for Normal Operating Condition	34
4-10	Temperature Distribution for Long Term Accident Condition	35
4-11	Temperature Distribution for Hydrogen Burning Condition	36
4-12	Accumulated Plastic Strain in Liner, Median Pressure Capacity for Long Term Accident Condition	38
4-13-	Maximum Principal Concrete Strains, Median Pressure Capacity for Long Term Accident Condition	39
4-14	Accumulated Plastic Strain in Hoop Tendons, Median Pressure Capacity for Long Term Accident Condition	40
4-15	Accumulated Plastic Strain in Liner, Median Pressure Capacity for Normal Operating Condition	41
4-16	Maximum Principal Concrete Strains, Median Pressure Capacity for Normal Operating Condition	42
4-17	Accumulated Plastic Strain in Hoop Tendons, Median Pressure Capacity for Normal Operating Condition	43
4-18	Accumulated Plastic Strain in Liner, Median Pressure Capacity for Hydrogen Burning Condition	44
4-19	Maximum Principal Concrete Strains, Median Pressure	45

for Pressure Loads

---

	<b>Capacity for Hydrogen Burning Condition</b>	
<b>4-20</b>	<b>Accumulated Plastic Strain in Hoop Tendons, Median Pressure</b>	<b>46</b>
	<b>Capacity for Hydrogen Burning Condition</b>	
<b>4-21</b>	<b>Pressure Fragility with Temperature for PCCV Liner Tearing</b>	<b>50</b>
<b>4-22</b>	<b>Pressure Fragility with Temperature for PCCV Rebar Failure</b>	<b>50</b>
<b>4-23</b>	<b>Pressure Fragility with Temperature for PCCV Tendon Failure</b>	<b>51</b>
<b>4-24</b>	<b>Pressure Fragility with Temperature for PCCV Concrete Failure</b>	<b>51</b>

## **List of Acronyms**

The following list defines the acronyms used in this document.

<b>3-D</b>	<b>three dimensional</b>
<b>ACI</b>	<b>American Concrete Institute</b>
<b>ASME</b>	<b>American Society of Mechanical Engineers</b>
<b>CCW</b>	<b>component cooling water</b>
<b>DG</b>	<b>draft regulatory guide</b>
<b>ESWS</b>	<b>Essential Service Water System</b>
<b>LOCA</b>	<b>loss of coolant accident</b>
<b>PCCV</b>	<b>prestressed concrete containment vessel</b>
<b>PDF</b>	<b>probability density function</b>
<b>RCP</b>	<b>reactor coolant pump or reactor coolant main pipe</b>

## **1.0 SCOPE**

The analyses described herein are provided to establish the fragility of the US-APWR primary containment system for over-pressurization. Fragility is defined as the cumulative probability of failure for increasing internal pressure. Here, failure is taken to be a breach in the primary containment boundary, consisting of the steel lined PCCV walls and the operable penetrations, such as personnel airlocks and equipment hatches. Sufficient test evidence and experience exists to exclude the fixed penetrations, such as electrical, feed water, and steam lines, as the limiting components in the pressure capacity. A breach in the boundary can be caused from tearing of the steel liner, flange distortion at the bolted connections, tearing of the steel components in the penetrations, loss of anchorage for the penetrations, or a structural failure of the concrete walls away from the penetrations. Because excessive internal pressure is related to extreme accident conditions, this fragility is also a function of elevated temperatures, which develop in tandem with increasing pressure. The fragility is calculated for 3 specified thermal conditions, namely, steady state normal operating temperatures, steady state conditions representing long term accident conditions, and transient thermal conditions for a representative hydrogen burning condition involving much higher temperatures but for much shorter durations. This range of fragility with temperature can then be coupled in the probabilistic risk assessment with the hazard rates for the probabilities that these thermal conditions and the associated pressure levels will occur during the life of the plant.

## 2.0 SUMMARY DESCRIPTION

The fragility of the US-APWR primary containment system to over-pressurization under accident conditions is summarized in Table 2-1. This table provides the median value and a 95% High Confidence (HC) value for the failure pressures causing the various failure modes that lead to a breach in the containment boundary. Figures 2-1, 2-2, and 2-3 plot the fragilities for these failure modes for normal operating, long term accident, and hydrogen burning thermal conditions, respectively.

The analyses indicate that the pressure capacity is limited by liner tearing, which is found to first initiate at the transition to the thickened concrete section for the equipment hatch. The expected or median pressure to initiate tearing is found to be 223.6 psig or 3.29 times the design pressure (Pd) of 68 psig for the steady state thermal conditions associated with a long term accident condition. This limitation in pressure capacity due to liner tearing is consistent with the ¼ scale PCCV tests performed at Sandia National Labs, References 5.3.17 and 5.3.18. The 95% confidence value for liner tearing under long term accident conditions is determined to be 176 psig or 2.59\* Pd in these analyses. The median capacity due to liner tearing for the hydrogen burning case is found to be 238.5 psig or 3.51\* Pd. This pressure is higher than that at normal operating conditions, which is attributed to the compressive stress induced into the liner due to the locally higher temperatures of the liner relative to the concrete. However, note that the 95% HC value for pressure capacity due to liner tearing under hydrogen burning conditions is lower than that for normal operating conditions reflecting the additional uncertainty for the severe accident conditions and effects of high temperatures.

For ultimate capacity based on rebar and tendon rupture, the median pressure capacity for long term design accident conditions is found to be 243.6 psig or 3.58\* Pd . It is also determined that the ultimate capacity is not limited by the concrete strength. These results are again consistent with the SNL test for the ¼ scale PCCV model. These analyses also indicate that the ultimate capacity does not strongly depend on temperature. The median ultimate capacity at normal operating temperature is determined to be 3.65\*Pd and the median ultimate capacity under hydrogen burning conditions is 3.60\*Pd.

**Table 2-1  
Summary of US-APWR Fragility for Over-Pressurization**

Failure Mode	Failure Pressure Pressure (psig) Followed by Factor on P <sub>d</sub>					
	Normal Operating Conditions		Long Term Accident Conditions		Hydrogen Burning Conditions	
	Median	95%HC	Median	95%HC	Median	95%HC
PCCV Liner Tearing	230.0	184.9	223.6	176.0	238.5	183.7
	3.38	2.72	3.29	2.59	3.51	2.70
PCCV Rebar Rupture	250.0	195.9	243.6	187.2	244.5	184.2
	3.68	2.88	3.58	2.75	3.60	2.71
PCCV Tendon Rupture	248.0	200.7	243.6	192.9	249.0	192.9
	3.65	2.95	3.58	2.84	3.66	2.84
PCCV Concrete	252.0	203.7	255.6	202.2	255.7	197.9
	3.71	3.00	3.76	2.97	3.76	2.91

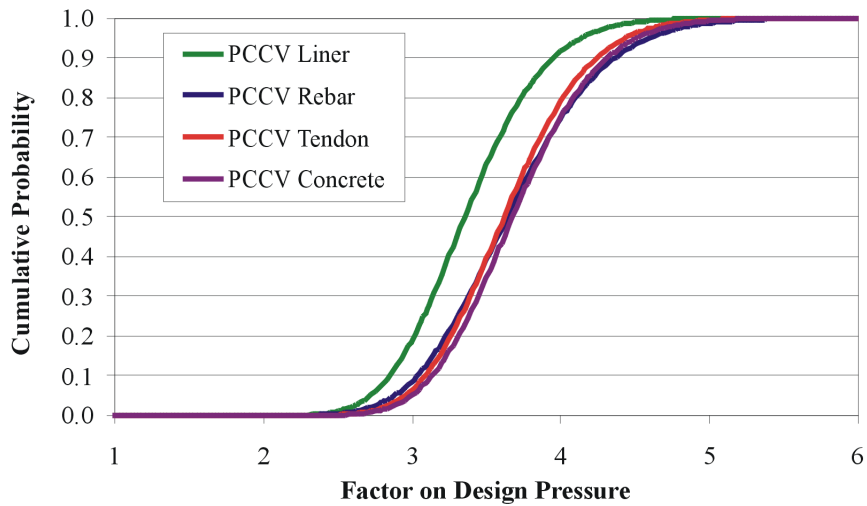


**Figure 2-1 Pressure Fragility under Normal Operating Thermal Conditions (105 °F)**

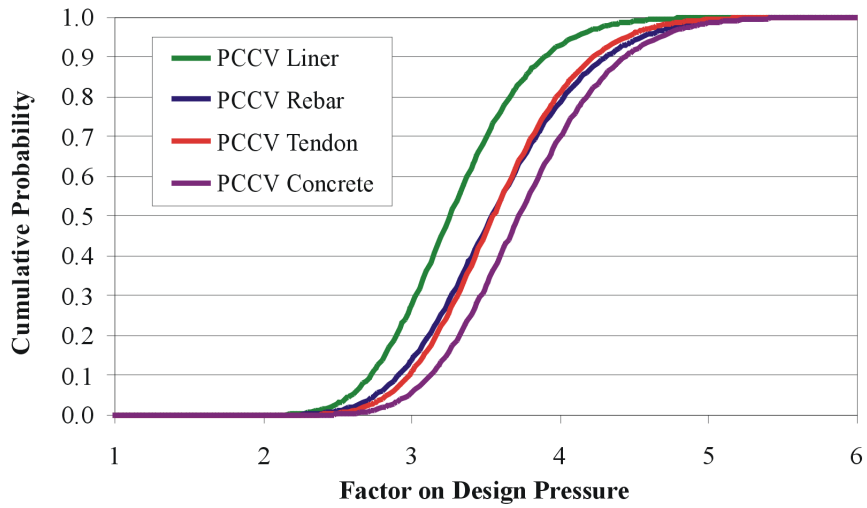


Figure 2-2 Pressure Fragility under Long Term Accident Thermal Conditions (438 °F)

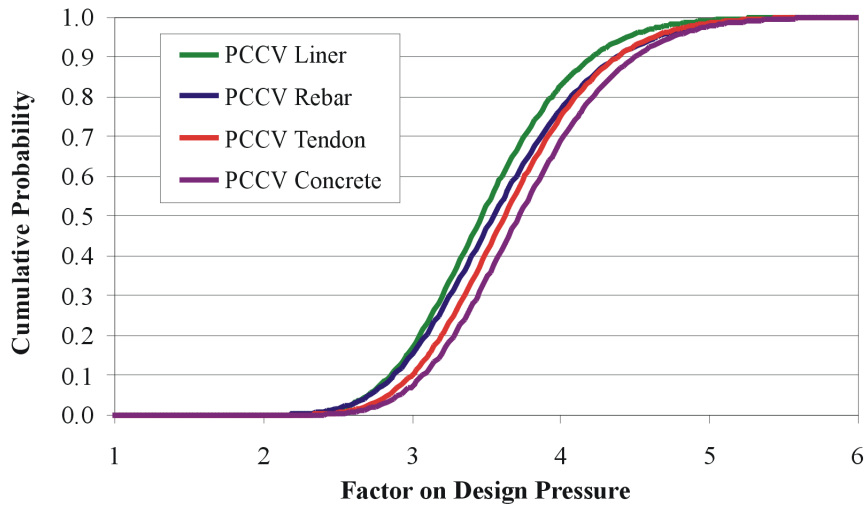


Figure 2-3 Pressure Fragility under Hydrogen Burning Thermal Conditions (1000 °F)

### **3.0 ANALYSIS METHODS**

These analyses use the ABAQUS/Standard finite element computer program, Reference 5.3.1, coupled with the ANACAP-U concrete constitutive model, Reference 5.3.2. This software has been used in similar previous work for reinforced concrete containments, Reference 5.3.10.

These analyses are based on detailed 3D finite element modeling, advanced material constitutive relations including material degradation with temperature, and an assessment of uncertainties within a probabilistic framework. The uncertainties in the analysis results are associated with the finite element modeling (such as mesh fidelity and constitutive modeling), material properties of the in-situ structure at the time of the over-pressurization, failure criteria or limit states used in establishing pressure capacity, and loading conditions that lead to pressurization of the containment. The uncertainties are evaluated by first identifying those parameters that are likely to have a significant effect on the analysis results and then evaluating the effect of variations in these parameters using the 95% confidence value of the specific parameter while keeping all other parameters at the median values. In some cases, such as material property variations, additional analytical calculations are needed to evaluate the uncertainty. In other cases, such as variation in failure criteria, re-evaluation of existing analyses can be performed. By assuming that the structural response is best characterized by a lognormal probability density function (PDF) for variations in these parameters (as allowed in DG-1203, Reference 5.3.20), the standard deviation or variance for the lognormal distribution for each important parameter is determined. The overall variance is determined by using a square root of the sum of the squares combination of the lognormal deviations for the individual parameters. Having the median value and lognormal deviation for the pressure capacity, a cumulative probability of failure for increasing pressure is established by integrating the lognormal probability density function.

Accident conditions leading to over-pressurization will also include elevated temperatures. Because of thermal induced stresses and material property degradation at elevated temperatures, the fragility for over-pressurization is also a function of temperature. Thus, the fragility analyses are conducted for three different thermal conditions, 1) normal operating steady state conditions, 2) a long term accident condition, and 3) a hydrogen burning condition. For the long term accident condition, the temperature distribution is based on a steady state condition where the PCCV atmosphere has reached 438 °F over about 120 hours representative of a bounding LOCA event. For the hydrogen burning condition, the temperature distribution for the pressure capacity is based on a transient thermal condition using a snapshot of the temperatures when the PCCV liner reaches 1000 °F in a few seconds due to a hydrogen burn scenario. These thermal conditions are described in more detail in Section 3.6 below.

#### **3.1 Finite Element Modeling**

Failure of the containment is defined here as a breach in the containment boundary, which can occur as a result of structural failure in the PCCV walls, liner tearing at discontinuities, such as anchorages or thickened plates at penetrations, tearing in the steel components of the penetrations, or due to distortion of the bolted flanges in the closure connections of the operable penetrations. A global, 3D finite element model is used to determine the pressure capacity of the PCCV structure assuming no leakage or failure in the steel penetration components. Previous work and experimental data, References 5.3.17 and 5.3.18, indicate that liner tearing will likely constitute the limiting component for pressure capacity in the

primary containment system.

A full 3D global model is used as the basis for establishing the pressure capacity of the PCCV. Because of the equipment hatch and other penetrations with thickened concrete sections, the containment structure does not have a true plane of symmetry. The thermal conditions leading to over-pressurization are also not symmetric around the containment due to partial coverage of the PCCV by the reactor building. The model is free standing and includes a portion of the basemat for anchoring the axial tendons. Continuum (solid) elements with embedded truss-like sub-elements for the reinforcement are used for the reinforced concrete sections. Truss elements with appropriate constraints to the concrete are used for the axial and hoop tendons. Plate elements are used for the steel liners and the penetration sleeves. In this global model, these liner elements are “glued” to the concrete surfaces without explicitly modeling the anchorage system. The global model includes representations for the equipment hatch, personnel lock, and fuel transfer tube penetrations, but the global analysis is performed assuming that leakage does not occur in these components.

Each analysis requires a thermal and a stress version of the model. The thermal model is used to determine the temperature distribution within the structure for each of the 3 thermal conditions, and the stress model is used to determine the pressure capacity based on the temperature distribution of interest and the combinations of the other parameter values. The temperature distributions are assumed to be independent of the stress solution, that is, the temperatures do not depend on displacements. The thermal analyses use bi-linear 8-node brick elements to avoid convergence issues associated with bi-quadratic elements and the implicit formulation used in the thermal solution. Steady state temperature solutions are used for the normal operating and long term accident cases. A transient thermal solution is used for the hydrogen burning case with the initial conditions set to the steady state operating conditions. The appropriate temperature distribution is then transferred to the stress model, and the internal pressure is incrementally increased to find the failure pressure with that temperature distribution. The stress analyses use bi-quadratic (20-node) brick elements with reduced Gaussian quadrature integration. From past experience, these elements perform the best for concrete cracking analyses for a given level of mesh refinement or nodal degrees of freedom. Thus, the thermal analyses use models with 8 times as many elements, where each 20-node, quadratic element is divided into eight 8-node linear elements. The temperature distributions at the nodes for the specified time points are read into the stress analysis from the thermal models. The stress analysis is based on static equilibrium, ignoring inertia effects. At each of the load increments for increasing internal pressure, equilibrium iterations are used to redistribute the loads and section stresses as cracking develops. The stress analyses are then evaluated per the failure criteria described in Section 3.9 below to establish the failure pressure.

### **3.2 Loading Conditions**

The analyses are performed by initializing the stress solution to be stress free at a uniform ambient temperature of 70 °F (21.1 °C) and then applying gravity loads and tendon prestressing. A thermal analysis (either steady state or transient, as appropriate) is performed to establish the temperature distributions within the structure for each particular thermal condition. The temperature distribution and pressures corresponding to that temperature condition are then incrementally applied to the stress model. Finally, the internal pressure is then slowly increased with static equilibrium iterations, holding the temperature distribution constant, to determine the pressure at which failure or leakage occurs for that

thermal condition and combination of material and parameter values.

### 3.3 Probabilistic Assessment

The analytical procedure used to develop the fragility, defined as the cumulative probability of failure for increasing pressure, for the various temperature conditions is summarized as follows.

1. Determine the pressure capacity ( $P_m$ ) using median values of all material properties and other conditions having significant influence on the structural capacity. This requires definition of various failure criteria or limit states, such as rupture strain in rebar or shear strain across concrete sections, as discussed in Section 3.9. This median pressure capacity will also use the median values for these failure criteria.
2. For all material or structural limit states used as failure criteria in judging the ultimate pressure capacity, a median value of the limit state and a value having a  $-1.645$  standard deviation (95% confidence level for the value) are defined. For each of these failure criteria, the pressure capacity is evaluated using the 95% confidence value together with the median values for all other failure conditions. The logarithmic standard deviation for the pressure capacity due to variation in the failure criteria is then calculated as,

$$\beta_f^i = \frac{\text{Ln}(P_f^i / P_m)}{-1.645}$$

where  $P_f^i$  is the pressure capacity when evaluated using the 95% confidence value for the  $i^{\text{th}}$  failure criteria. The assumptions are that the natural logarithm of the failure pressure has a normal distribution for variations in the parameters, and that all the parameters considered are independent of each other. Note that several values of  $P_m$  are calculated in Step 1 corresponding to different failure modes or limit states of various components. The appropriate median pressure associated with the capacity for the failure criteria under evaluation is used to determine the standard deviation for that parameter.

3. For all material properties having significant influence on the structural pressure capacity, a median and 95% confidence value are defined. These parameters are discussed further in Section 3.4 below. An additional analysis with the appropriate model is performed for each of these parameters using the 95% confidence value for the parameter under consideration and with median values for all other parameters, including the failure criteria. The logarithmic standard deviation for the pressure capacity due to variation in these parameters is then calculated as,

$$\beta_s^i = \frac{\text{Ln}(P_s^i / P_m)}{-1.645}$$

where  $P_s^i$  is the pressure capacity when evaluated using the 95% confidence value for the  $i^{\text{th}}$  parameter or material property. Again the median failure pressure associated with the parameter under investigation is used in this equation.

4. Assign a logarithmic standard deviation for the pressure capacity due to modeling uncertainties ( $\beta_m$ ), including such things as mesh refinement, constitutive modeling, geometric tolerances, and manufacturing/construction imperfections. This variance for

uncertainty is developed using comparisons of analytical predictions to test data results using similar modeling techniques from past work. This is discussed further in as discussed in Section 3.5 below.

5. Calculate a composite lognormal standard deviation for the pressure capacity as the square root of the sum of the squares of all individual standard deviations, as

$$\beta = \sqrt{\sum (\beta_f^i)^2 + \sum (\beta_s^i)^2 + \beta_m^2}$$

6. Steps 1-5 are performed only for the “median” temperature condition, identified as the steady state long term accident case. The lognormal standard deviations so computed are then used in evaluating the fragility for the other temperature cases. The median pressure capacity for the other temperature cases is calculated using the median values of all parameters but under the temperature distributions corresponding to the temperature condition specified. The assumption here is that the uncertainty in the analyses does not change significantly for the different thermal conditions. Only the median pressure capacity is significantly affected by the temperature condition. This is to bring the computational effort in line with the level of effort needed for the scope of the project.
7. The fragility will be based on a lognormal probability density function (Reference 5.3.19) for the failure pressure defined as

$$p_f(p) = \frac{1}{p\beta\sqrt{2\pi}} \exp\left[-\frac{1}{2}\left(\frac{\ln(p/P_m)}{\beta}\right)^2\right] \text{ for } p > 0, \text{ and } p_f(p) = 0 \text{ otherwise,}$$

where  $p$  is the failure pressure,  $P_m$  is the mean value of failure pressure, and  $\beta^2$  is the variance of the normally distributed natural log of  $p$ . The cumulative probability or fragility is determined from integration of the probability density function, so that the probability that the failure pressure is less than  $\bar{P}$  is defined by

$$P = \int_0^{\bar{P}} p_f(p) dp .$$

### 3.4 Uncertainty in Parameter Variability

To address aleatory uncertainty associated with variability of parameters for which a range of values can be determined, variations in key analysis parameters are considered. The following parameters are identified as significant in affecting the calculated structural capacity for internal pressure and requiring an evaluation of the uncertainty involved.

- $f_c'$  Concrete compressive strength. This also affects the concrete stiffness (modulus), shear performance, and cracking characteristics. This is deemed an important material variable in determining the pressure capacity of the PCCV from the global modeling.
- $F_T^{conc}$  The factor for degradation of concrete material properties with increasing temperature. This is considered an important material modeling variable in determining the pressure capacity of the PCCV from the global modeling.
- $\sigma_y^{rebar}$  Yield stress for rebar. This is deemed an important material variable in determining the pressure capacity of the PCCV from the global modeling.

Generally, variations in yield stress also correspond to changes in ultimate tensile strength.

- $\sigma_y^{steel}$  Yield stress for the steel components, again with some corresponding variation in tensile strength. This is deemed an important material variable in determining the pressure capacity of the steel components.
- $\sigma_y^{weld}$  Yield stress (and tensile strength) of welded joints. This could affect the failure pressure in the equipment hatch modeling. Variations in this parameter will be accounted for in determining the 95% confidence band for the rupture strain in assessing the failure of components with welded joints.
- $F_T^{st}$  The factor for degradation of steel material properties with increasing temperature, but is deemed a small effect relative to the 95% confidence value that will be applied to the yield stress, that is, the effect of temperature on yield stress is not that significant (~82.5% of median at 500 °F). Variations for this parameter will be considered in determining the 95% confidence value for yield stress.
- $\sigma_{pre}^{tendon}$  Level of prestressing in PCCV concrete. This is deemed an important parameter in determining the pressure capacity of the PCCV from the global modeling. Variations will include the effects of tendon relaxation, concrete creep, and loss at anchorages. The 95% confidence value will be based on the 50 year value of pre-stressing used in the design of the PCCV.
- $\sigma_y^{tendon}$  Yield stress (and tensile strength) of the tendons. This is considered an important material variable in determining the pressure capacity of the PCCV from the global modeling.
- $\sigma_y^{bolt}$  This is the yield strength for the bolts in the bolted connections in the equipment hatch. This is a material parameter used for establishing the failure pressure for leakage at the bolted connection.
- $\sigma_{pre}^{bolt}$  This is the pre-stress in the bolts for the bolted connections in the equipment hatch. This parameter can affect the pressure capacity due to flange distortion.
- $\epsilon_r^{reb}$  The level of plastic strain used to define rupture of rebar. This is an important failure criteria parameter, and will be considered as a parameter variation to determine a corresponding  $\beta_f$ . The rebar rupture strain is determined by factoring uniaxial test data to account for strain concentrations at concrete cracks, which is below the refinement level of the analytical model.
- $\gamma_s^{conc}$  The level of shear strain across a section of pre-stressed concrete causing shear failure of the section. This is an important failure criteria parameter in establishing shear capacity, and will be considered as a parameter variation to determine a corresponding  $\beta_f$ .
- $\epsilon_r^{st}$  The level of effective plastic strain used to define failure of structural steel components, and is factored from uniaxial test data to account for mesh refinement and biaxial loading. This is deemed an important failure criteria parameter for which a  $\beta_f$  will be determined.

---

**for Pressure Loads**

---

- $\epsilon_r^{liner}$  The level of effective plastic strain used to define tearing in steel liner material, determined by factoring uniaxial test data to account for mesh refinement and biaxial loading. This is a failure criteria parameter, and will be lumped with SCF below in determining a standard deviation for uncertainty. Reduced ductility due to welding of the liner will also be taken into account in developing the 95% confidence value.
- SCF This is a strain concentration factor to evaluate liner tearing at liner discontinuities, such as anchorages, that are not included in the model. This will be derived based on previous work. This is a failure criteria parameter to be lumped with the tearing strain level above to determine a standard deviation for liner tearing.
- $\epsilon_r^{tendon}$  The level of plastic strain used to define rupture of tendons. This is an important failure criteria parameter, and will be considered as a parameter variation to determine a corresponding  $\beta_f$ .

### 3.5 Uncertainty in Modeling and Processes

There is also epistemic uncertainty associated with unknown processes and the modeling and analytical limitations used in the analyses for determining the failure pressures for any given set of material properties, geometry, or other problem parameters. This uncertainty concerns the mesh fidelity, the type of element formulations used, the robustness of the constitutive models, the equilibrium iteration algorithms and convergence tolerances, geometric imperfections, construction exactness, rebar placement locations, and the like. This modeling uncertainty must be quantified as part of the fragility calculation. Generally, this uncertainty is based on experience and judgment of the analyst because the analytical effort needed to consider variations in these modeling parameters is prohibitive. However, for this effort, some engineering judgment is invoked, but the modeling uncertainty is primarily based on previous work where similar modeling has been used to predict structural performance that can be compared to test data. This procedure has been employed in similar previous work, Reference 5.3.10. Several pretest analytical predictions have been performed for structural specimen tests using the same software and modeling philosophy, namely mesh fidelity, element formulations, convergence algorithms, and so forth. Many of these predictions and tests concern the pressure capacity of concrete containments, for example, the 1:4 scale PCCV model tested to over-pressurization failure at Sandia National Laboratories, References 5.3.17 and 5.3.18. Thus, the modeling uncertainty can be determined by comparing the predicted analysis results with the test results. A list is constructed of about 20 such comparisons, and the ratio of the test result to the predicted result is determined for each. These data points are sorted into ascending order and plotted for cumulative probability versus the ratio of test result to analysis prediction. The cumulative probability is then calculated for each point as  $n/(N+1)$  where  $n$  is  $n$ th point in the series and  $N$  is the total number of data points. For example, the probability that the test-to-analysis ratio will be less than that defined by the  $n$ th point is  $n/(N+1)$ . A cumulative probability function, based on a lognormal probability distribution function, can then be fitted to the data through a least squares analysis for the 2 parameters defining the lognormal PDF. This is illustrated in Figure 3-1, and the so determined lognormal variance is the uncertainty in the modeling used for these analyses. Note that the mean for the fitted lognormal PDF is a measure of the shift from a ratio of 1.0 for the test results to the analysis predictions. The calculated value shows that the analysis predictions are in general slightly smaller than the test results, i.e. that the median value of the ratio is 1.004. This means that a calculated median failure pressure is likely to be slightly below the actual value for the modeling procedures employed. Therefore, the modeling

techniques employed are comfortably accurate and, if anything, are slightly conservative. Because the test data and analyses are all at ambient temperatures, the calculated  $\sigma$  for modeling uncertainty is increased by 10% for the analyses associated with the long term accident thermal conditions and by 20% for the analyses of the hydrogen burning thermal conditions. The values of lognormal standard deviations for modeling uncertainties are summarized in Table 3-1.

**Table 3-1**  
**Summary of Variance for Modeling Uncertainty**

Analysis Type	Lognormal Standard Deviations		
	Normal Operating	Long Term Accident	Hydrogen Burning
Global Modeling	.1232	.1355	.1478

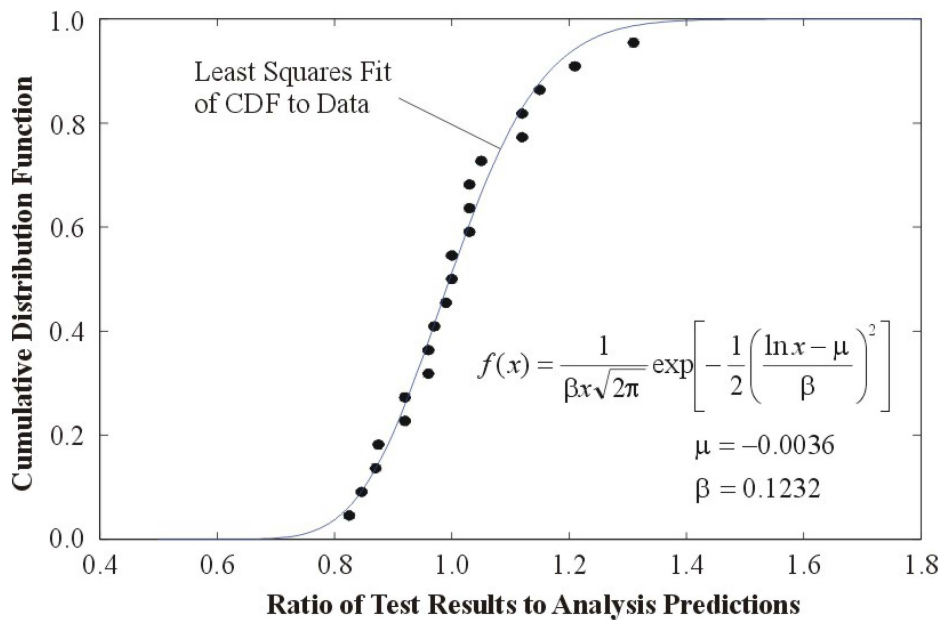


**Figure 3-1 Calculation of Variance due to Modeling Uncertainty**

### 3.6 Thermal Conditions

As mentioned above, the fragility to over-pressurization is a function of temperature because internal pressure is associated with an accident condition involving elevated temperatures, and the capacity also depends on thermal stresses and material property degradation at elevated temperatures. The variation and uncertainty in the thermal conditions is considered here by defining a range of thermal conditions used in determining the fragility. The thermal conditions are intended as bounding cases for the type of accident under consideration. The associated probability of failure with pressure level can then be evaluated in the risk assessment by considering the probability that a given internal pressure can exist for a given thermal condition and the probability that the combination will occur during the life of the structure.

The pressure capacity is thus calculated at 3 different thermal conditions, 1) normal operating steady state conditions, 2) steady state long term accident conditions, and 3) hydrogen burning transient conditions where high temperatures develop for a short duration. These thermal conditions are assumed to develop in extreme winter ambient conditions where larger thermal gradients through the structure would develop, as a conservative measure to help minimize the number of analyses needed. The interior of the PCCV has uniform atmospheric temperature that acts over all interior surfaces. The exterior of the PCCV has some surface area exposed to ambient (open air) temperatures and some surface area exposed to room temperatures where the reactor building covers parts of the PCCV. These areas for the exterior surface of the PCCV are defined in Figure 3-2. The actual boundaries in the model are approximate based on element sizing and spacing. The interior surfaces of the penetration collars through the PCCV wall will also be exposed to room temperatures because these are covered by the reactor building, and the closure lids for the penetrations are on the inside of the containment. The inside surface of the closure lid and flanges are exposed to the PCCV atmosphere temperature. Table 3-2 provides a summary of the temperature conditions for the various surfaces for the 3 thermal conditions based on Reference 5.1.1. The film coefficients to be used for heat convection on the various surfaces, as summarized in Table 3-5, are based on relations taken from Reference 5.3.21.

The PCCV interior atmosphere temperature representing the long term accident is based on the data for loss of coolant in LOOP or CCW/ESWS and RCP seal LOCA with failure of any mitigation functions, as described in Reference 5.1.2. A simplified fit to this data is provided in Table 3-3 and plotted in Figure 3-3. For this thermal condition, the temperature distribution is based on a steady state solution with the PCCV atmosphere at 438 °F, which develops around 100 hours. The conditions for the hydrogen burn, which are also referred from Reference 5.1.2, are based on the conditions with transient temperature and pressure change in relation to hydrogen burn. Table 3-4 provides the tabular data for this hydrogen burning condition with the corresponding plot in Figures 3-4. The temperature distribution for this case is specifically assumed for this containment performance study based on a transient thermal analysis with a snapshot of the temperature distribution taken when the liner reaches 1000 °F.

**Table 3-2**  
**Summary of Temperature Conditions**

<b>Condition</b>	<b>PCCV Interior Temperature (°F)</b>	<b>PCCV Open Air Temperature (°F)</b>	<b>PCCV Room Temperature (°F)</b>	<b>Ground<sup>a</sup> Temperature (°F)</b>
Normal Operating Steady State	105	-40	50	35
Long Term Accident Steady State	438	-40	50	35
Hydrogen Burn Transient	1000	-40	50	35

<sup>a</sup>The ground temperature is the temperature assumed at the bottom of the basemat.

**Table 3-3**  
**Temperature and Pressure in PCCV for Long Term Accident Thermal Condition**

**Table 3-4**  
**Temperature and Pressure in PCCV for Hydrogen Burning Thermal Condition**

**Table 3-5**  
**Film Coefficients for Thermal Conditions**

<b>Surface</b>	<b>Film Coefficient (BTU/hr-ft<sup>2</sup>-°F)</b>	<b>Comments</b>
Interior Steel Surfaces	infinite	Use large coefficient so that temperature of steel surface tracks PCCV atmosphere temperature
Exterior Concrete Surfaces	2.5	Concrete exposed to ambient elements and wind
Interior Concrete Surfaces	1.0	Concrete exposed to controlled room circulation inside Reactor Building

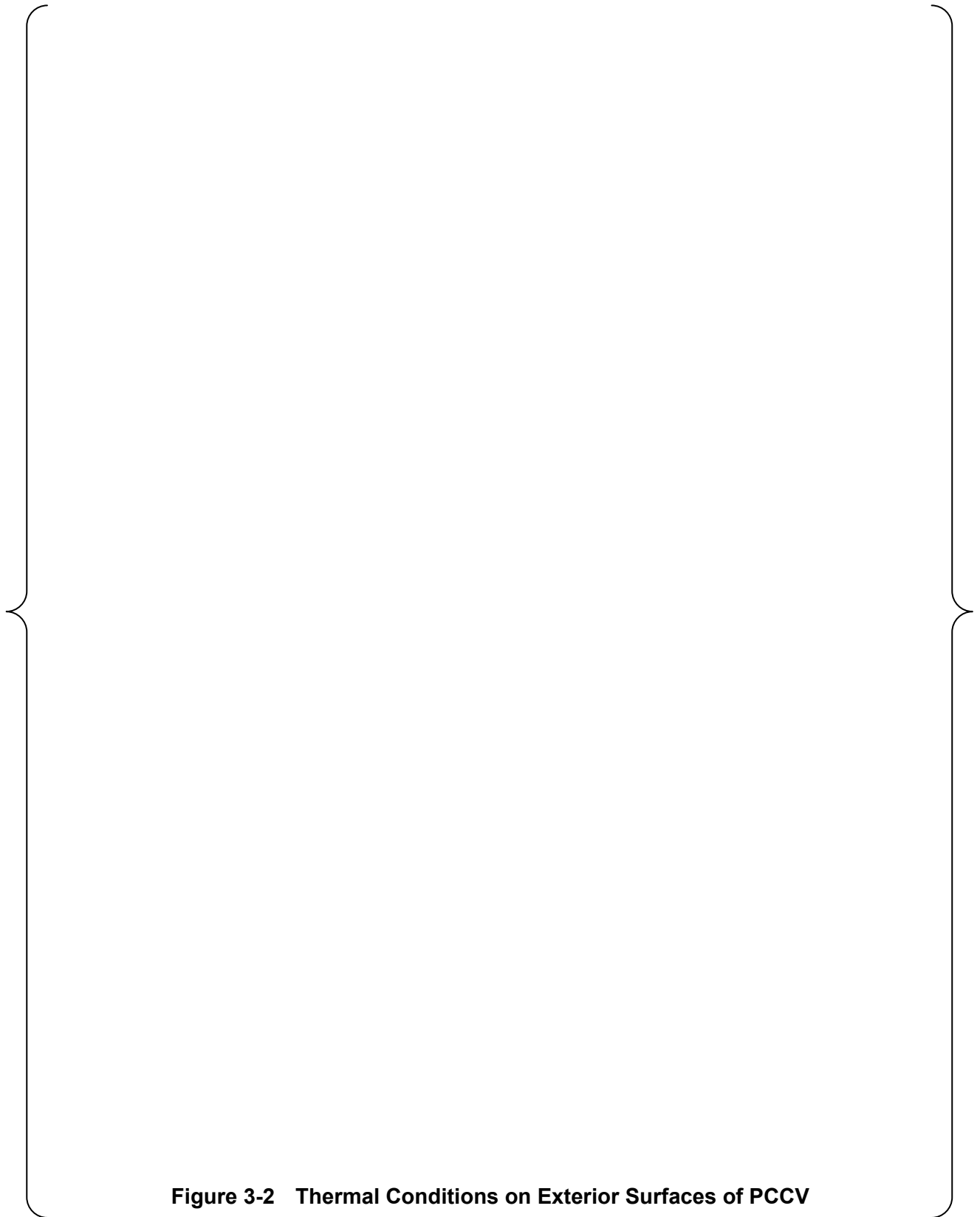


**Figure 3-2 Thermal Conditions on Exterior Surfaces of PCCV**

**Figure 3-3 Temperature and Pressure for Long Term Accident Condition**

**Figure 3-4 Temperature and Pressure for Hydrogen Burning Condition**

### 3.7 Material Properties

The analyses for establishing the pressure fragility of the primary containment system are best estimate calculations and are based on median or expected material properties. Analyses using the 95% confidence value of important material properties are used to assess the effect of uncertainty in the actual material properties. As described above, the variation in the thermal conditions leading to over-pressurization is handled by defining the fragility at various thermal conditions that are chosen a-prior to cover the temperature regimes of interest. Thus, variations in the thermal material properties are not considered in the uncertainty evaluation, for example, variations in the thermal conductivity or film coefficients will have little effect on the steady state temperature distribution through the PCCV wall for a given thermal condition where interior and exterior temperatures are defined. The thermal properties are based on commonly accepted values and summarized in Table 3-6. The heat transfer or film coefficients used for heat convection from surfaces exposed to temperatures are summarized in Table 3-5 in Section 3.6.

By contrast, the mechanical material properties and their variation with temperature can have a significant effect on determining the pressure capacity. The strength, stiffness, and shear capacity of concrete along with the yield stress and ultimate strength of reinforcement and tendons will directly affect the pressure resisting capacity of the PCCV. The yield stress, strain hardening characteristics, and ductility of the steel material will directly affect the performance of the liner and penetration components. Thus, median and 95% confidence values must be developed for the elastic and plastic material properties, all as a function of temperature. While a set of 3 discrete thermal conditions are identified for the range of temperatures of interest, the temperatures within the structural components will have a continually varying distribution. Thus, the material properties must cover the entire range of temperatures from ambient to 1000 °F. A summary of the snapshot values for 3 discrete temperatures are provided in Table 3-7 for the elastic properties and Table 3-8 for the plastic properties for the steel materials. This data has been collected and synthesized from a variety of sources, as noted in the tables. Typically, data for the median and distribution of a property at room temperature is available, and some data for the variation of the median value with temperature is found. The 95% confidence values at elevated temperatures are then determined using the distribution at room temperature but with increasing uncertainty for increasing temperature. For the steel materials, continuous curves for the effective stress versus effective strain plasticity relations are developed for both the median and 95% confidence values and for temperatures of 150, 250, 500, 800, 1000 °F. In the analysis, linear interpolation between these values is used for intermediate temperatures, so these temperatures are chosen to provide a relatively good piecewise linear fit to the degradation shapes of the properties with temperature. Figure 3-5 illustrates the engineering stress strain relations with temperature for A615 Grade 60 reinforcing bars for median and 95% confidence values. Figure 3-6 illustrates the engineering stress strain relations with temperature for A516 Grade 60 material used for the liner plate for both median and 95% confidence values.

For concrete, the elastic modulus, shear modulus, and tensile strength are functions of the compressive strength. The 95% confidence value for the compressive strength is taken as the design strength, namely 7 ksi concrete for the PCCV and 4 ksi concrete for the basemat. Because this should be the minimum value delivered in the field, the median value for compressive strength is based on the ACI requirements (Ref 5.2.3) linking the delivered strength to cylinder specimen testing accounting for variability. One requirement is that the average 28-day test cylinder strength,  $f'_c$ , exceed the specified design strength by the

## for Pressure Loads

amount  $1.34*s$ , where  $s$  is the standard deviation of the strength for the set of test specimens. Another requirement is that the cylinder test strength equal or exceed a value of  $0.9*f'_c + 2.33*s$ . The delivered strength is similar for these 2 requirements for coefficient of variations around 10% in the concrete batches. For the PCCV concrete, the 7 ksi design strength is based on the 90 day value, and the median value is determined using the same ACI relations. A variation of 10% in compressive strengths for any batch of concrete is assumed as a basis for deriving the standard deviation and calculating the median value of compressive strength at ambient temperature. From this median value of compressive strength, the elastic modulus is calculated from the ACI relationship,  $E = 57,000\sqrt{f'_c}$ . The variation of compressive strength and tensile strength with temperature are based the data in Reference 5.3.9. No aging effects, which will strengthen the concrete over time, are included in these analyses. A summary of the concrete properties at these discrete temperatures is provided in Table 3-9. The behavior of the compressive strength with temperature is illustrated in Figure 3-10.

**Table 3-6**  
**Summary of Thermal Material Properties**

<b>Material</b>	<b>Weight Density (lb/ft<sup>3</sup>)</b>	<b>Specific Heat (BTU/lb-°F)</b>	<b>Conductivity (BTU/hr-ft-°F)</b>	<b>Coefficient of Expansion (/°F)</b>
Concrete	150	0.21	1.0	5.5E-6
Carbon Steel Liner	490	0.11	31	6.5E-6
Structural Steel	490	0.11	31	6.5E-6
Reinforcement <sup>1</sup>	--	--	--	6.5E-6
Tendons <sup>1</sup>	--	--	--	6.5E-6

<sup>1</sup>Reinforcement and Tendons take on the temperatures of the surrounding concrete

**Table 3-7**  
**Summary of Elastic Mechanical Properties for Steels**

	Normal Operating Conditions (150 °F)		Long Term Accident Conditions (500 °F)		Hydrogen Burning Conditions (1000 °F)		Ref
	Median	95 %	Median	95 %	Median	95 %	
SA 516 Carbon Steel							
Modulus (xE6 psi)	29.5	29.0	26.8	26.4	17.7	17.4	5.2.2
Poisson's Ratio	0.289	0.289	0.295	0.295	0.304	0.304	5.3.6
Prestressing Tendons							
Modulus (xE6 psi)	28.6	28.4	26.9	26.4	25.2	24.4	5.3.8
Poisson's Ratio	--	--	--	--	--	--	

**Table 3-8**  
**Summary of Plastic Mechanical Properties for Steels**

	Normal Operating Conditions (150 °F)		Long Term Accident Conditions (500 °F)		Hydrogen Burning Conditions (1000 °F)		Ref
	Median	95 %	Median	95 %	Median	95 %	
SA516 Grade 70							
Yield Stress (ksi)	48.62	42.8	43.8	38.5	37.9	30.6	5.3.3
Tensile Strength (ksi)	77.04	71.3	70.9	66.7	63.6	50.8	5.3.4
Elongation (%)	20.3	17.0	20.5	16.4	33.7	24.0	5.3.5
SA516 Grade 60							
Yield Stress (ksi)	40.94	36.06	36.85	32.39	31.94	25.79	Based on Gr 70
Tensile Strength (ksi)	66.03	61.14	60.75	57.20	54.48	43.52	
Elongation (%)	25.1	21.0	25.4	20.3	41.7	29.7	
A615 Grade 60 Rebar							
Yield Stress (ksi)	68.6	63.5	54.9	45.7	39.1	29.0	5.3.6 5.3.7
Tensile Strength (ksi)	105.0	97.0	104.0	86.4	64.1	47.3	
Elongation (%)	12.5	8.6	13.0	9.0	14.0	10.0	
A416 Grade 1860 Tendons							
Yield Stress (ksi) @ 1%	259.5	243	249.1	231.0	233.5	212.1	5.3.8
Tensile Strength (ksi)	278.2	270	269.9	260.8	256.0	244.5	
Elongation (%)	3.66	3.50	3.80	3.60	4.00	3.74	

**Table 3-9**

**Summary of Concrete Material Properties**

Material/Property	Normal Operating Conditions (150 °F)		Long Term Accident Conditions (500 °F)		Hydrogen Burning Conditions (1000 °F)		Ref
	Median	95 %	Median	95 %	Median	95 %	
PCCV Concrete (7 ksi)							
Comp Strength (psi)	8891	7000	6757	5233	4817	3298	5.3.9
Strain at Peak Comp (%)	0.19	0.20	0.27	0.36	0.46	0.68	
Modulus (xE6 psi)	5.375	4.769	2.922	1.912	1.243	0.617	
Tensile Strength (psi)	707.2	627.5	537.4	416.3	383.1	262.4	
Fracture Strain (xE-6)	131.6	99.1	183.9	138.5	308.2	232.2	
Poisson's Ratio	0.22	0.18	0.22	0.18	0.22	0.18	
Basemat Concrete (4 ksi)							
Comp Strength (psi)	5081	4000	3818	2948	2722	1858	5.3.9
Strain at Peak Comp (%)	0.19	0.20	0.27	0.36	0.46	0.68	
Modulus (xE6 psi)	4.063	3.605	2.167	1.407	0.922	0.454	
Tensile Strength (psi)	534.6	474.3	401.7	310.1	286.4	195.5	
Fracture Strain (xE-6)	131.6	99.1	185.3	139.6	310.6	234.0	
Poisson's Ratio	0.22	0.18	0.22	0.18	0.22	0.18	

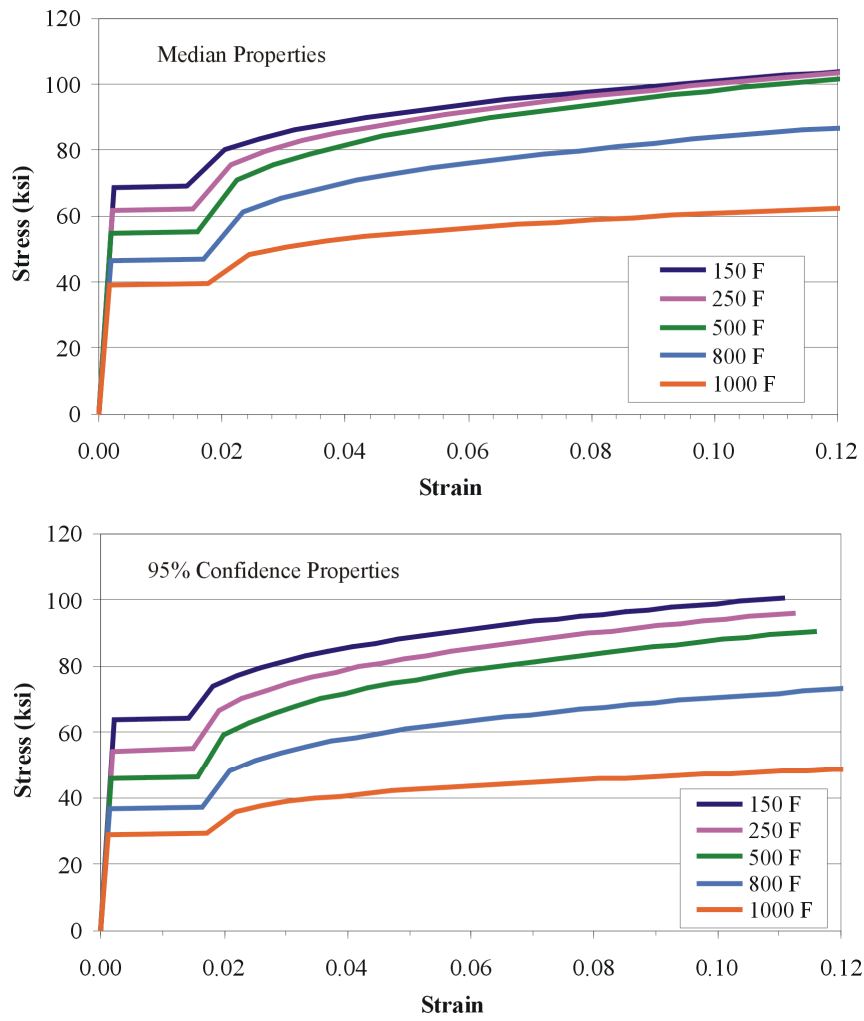
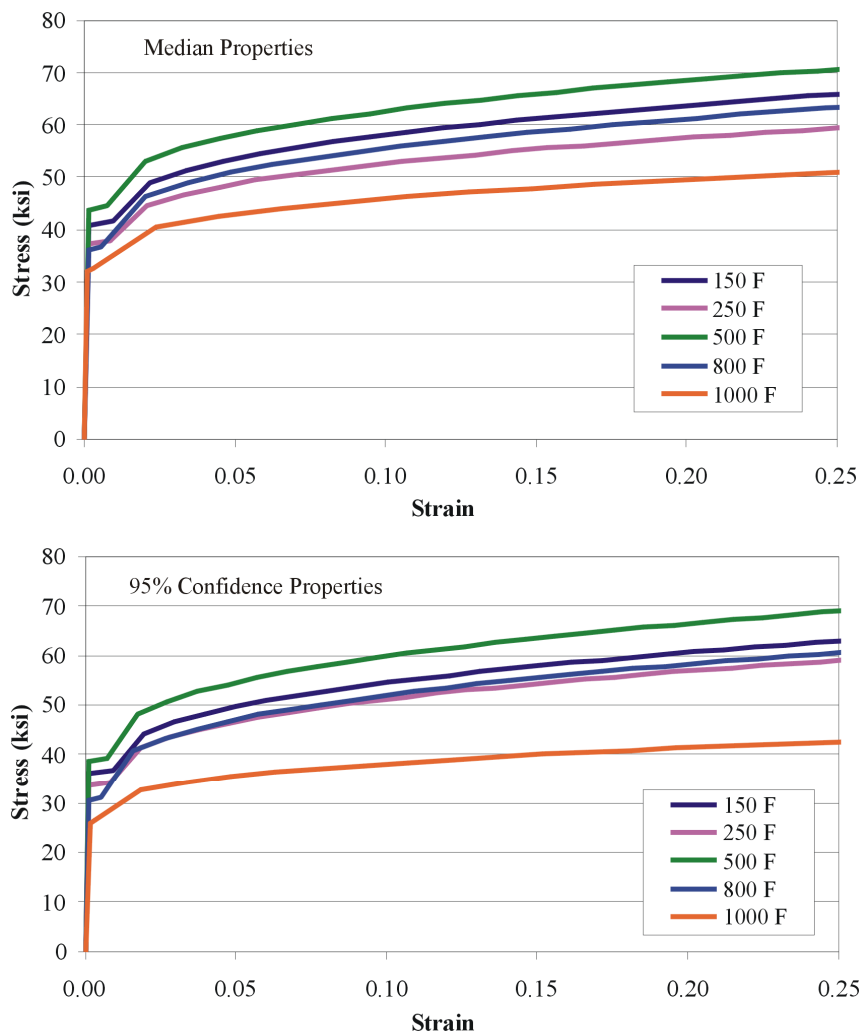


Figure 3-5 Illustration of Stress-Strain Relations for A615 Grade 60 Rebar



**Figure 3-6 Illustration of Stress-Strain Relations for A516 Grade 60 Liner Plate**

### 3.8 Concrete Performance

The modeling of the concrete is a key ingredient for the ultimate strength analyses and is provided through the ANACAP-U constitutive model. The behavior of concrete is highly nonlinear with a small tensile strength, shear stiffness and strength that depend on crack widths, and compressive plasticity. The main components of the concrete model for these analyses are tensile cracking, post-cracking shear performance, and compressive yielding when the compressive strength is reached. A summary description of the modeling for concrete behavior used in this software is described below.

Tensile cracking in the concrete is governed by the magnitude of the load in the directions of principal strain. Cracks are assumed to form perpendicular to the directions of largest tensile strains. Multiple cracks are allowed to form at each material point, but they are constrained to be mutually orthogonal. If cracking occurs, the normal stress across the crack is reduced to zero and the distribution of stresses around the crack is recalculated through equilibrium

iteration. This allows stress redistribution and load transfer to reinforcement or other load paths in the structure. Once a crack forms, the direction of the crack remains fixed and can never heal. However, a crack can close, resist compression and shear, and re-open under load reversals. The cracking criterion is based on an interaction of both stress and strain as illustrated in Figure 3-7. The model predicts cracking when the generalized (principal) stress and strain state exceeds the limit state shown. Thus, biaxial and triaxial stress states are treated consistently with uniaxial conditions, but the associated cracking will now occur at a slightly higher stress and slightly lower strain. Split cracking, for example near a free edge under high compressive stress, occurs at near zero stress and a tensile strain approximately twice that of uniaxial tensile cracking.

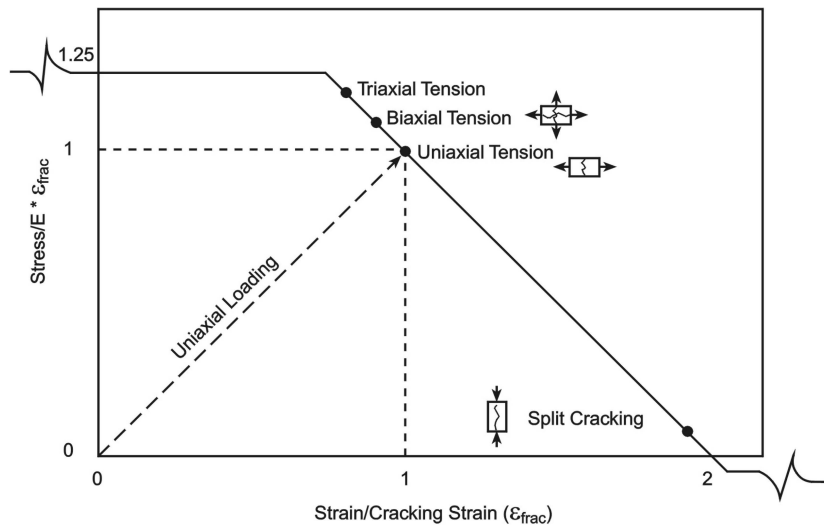


**Figure 3-7 Crack Initiation Criteria Curve**

The surfaces of cracks that develop due to tensile stress in concrete are usually rough and irregular. When a shear force is applied along a crack surface, tangential sliding occurs and this causes displacements normal to the crack surface to develop as the crack surfaces ride up on each other. When this normal displacement is restrained by reinforcement crossing the crack, tensile stresses will develop in the steel bars, which will then induce compressive stresses across the crack in the concrete. The resistance to sliding is provided by the frictional force generated by the compressive stress across the crack. The crack width is the primary variable affecting this mechanism of shear transfer. Smaller crack widths correspond to greater shear stiffness and strength. Aggregate size, reinforcement design, and concrete strength are other important factors. In order to account for the effect of cracking on shear stiffness, a reduced shear modulus is retained in the stress-strain matrix when a crack forms. The shear moduli in the plane of the crack are immediately reduced by 60% when a crack forms. The shear stiffness is further reduced using a hyperbolic variation with the opening strain normal to the crack, as illustrated in Figure 3-8.

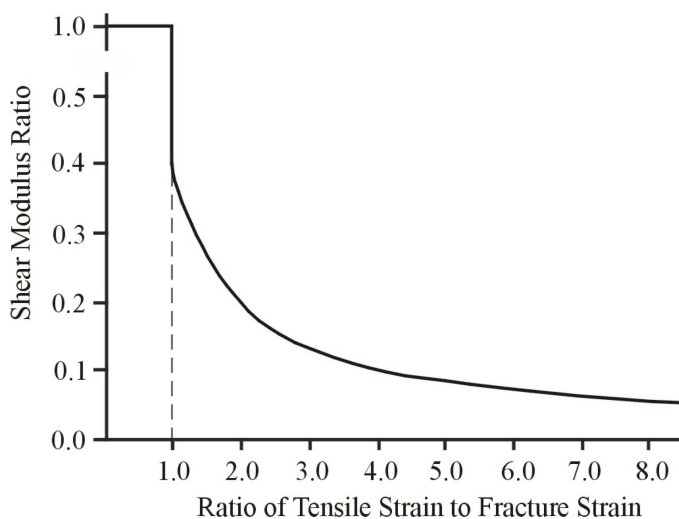


**Figure 3-8 Shear Modulus Reduction for Open Cracks**

Perhaps the most important feature of concrete modeling is the ability to capture the shear capacity in cracked concrete. The ANACAP model is equipped with a shear-shedding feature to model the shear stress capacity across an open crack. The shear retention model reduces the incremental shear modulus across an open crack as discussed above. The shear stress capacity for an open crack is a function of the crack opening strain, as illustrated in Figure 3-9. The shear-shedding feature reduces the shear stresses previously supported across an open crack if the crack continues to open. Again, equilibrium iterations are needed to redistribute the loads. Recall that cracks form in the principal strain directions so that, in general, there is no shear across a crack when it first opens. However, continued loading resulting in shear deformations will be carried in shear across the crack if possible.

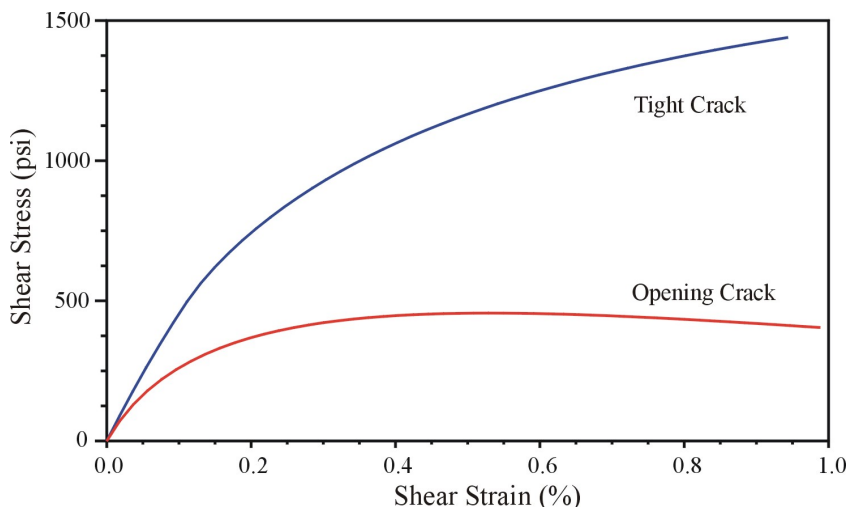


**Figure 3-9 Example of Shear Stress Capacity Across Open Cracks**

In the compression regime, the continuous stress-strain curve is defined from uniaxial test data, which is then generalized to multi-axial stress/strain states using the uniaxial equivalence of the multi-axial state, namely, the effective stress and the effective strain. The

for Pressure Loads

uniaxial behavior is generalized to multi-axial behavior, within the analytical framework of isotropic hardening plasticity formulation, using a Drucker-Prager surface to represent the loading surface under multi-axial compression. In this formulation, the loading surface is a function of the hydrostatic pressure, the second invariant of the deviatoric stress tensor, and the yield strength. This type of formulation incorporates the effects of low to moderate confinement stress levels, which typifies the behavior of civil structures. These relations allow for linear behavior for compressive stresses below about 50% of the compressive strength, and then strain hardening behavior until the compressive strength is reached. In addition, the compressive strength, initial modulus, and the compressive strain level that supports the peak compressive strength are functions of temperature. In compression, concrete softens with increasing temperature, exhibiting lower compressive strength while extending the range of competent compressive strain. The stress-strain behavior under uniaxial compression is illustrated in Figure 3-10, which shows both the median and 95% confidence properties for 7 ksi concrete.

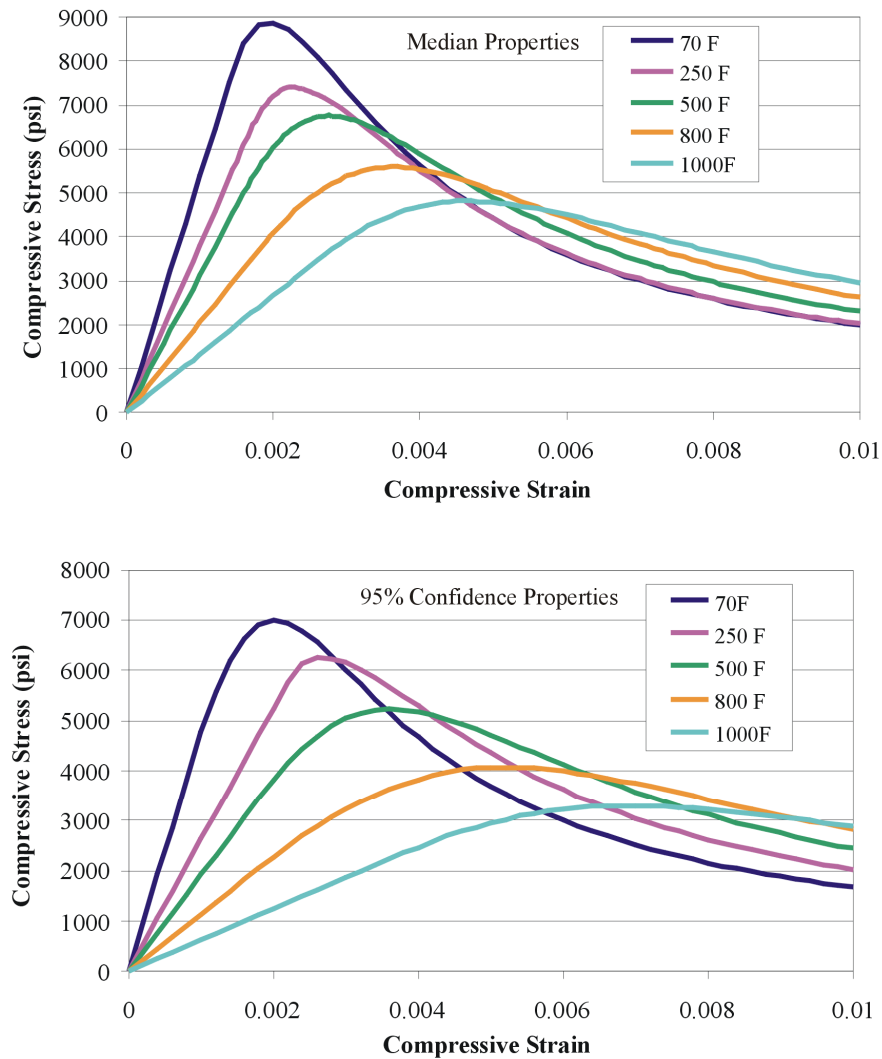


Figure 3-10 Uniaxial Compressive Strength as Function of Temperature

### 3.9 Failure Criteria

In evaluating the pressure capacity for the containment system, failure criteria must be defined to establish limit states on the structural response where the internal pressure is no longer contained by the structure. There is uncertainty in defining these failure criteria, so median and 95% confidence values are defined to evaluate the effect of the uncertainty on the analysis results. For the reinforced concrete components, failure either occurs when tensile loads cause rebars to yield and then rupture, or when the shear forces across a section exceed the shear capacity. Under bending loads, concrete crushing may develop on the compressive side, but failure of the section can still be attributed to rebar rupture on the tension side of the section. Section shear failure develops when sufficient cracking extends across a section such that the shear capacity of the concrete due to aggregate interlock is reduced below that needed to support the shear demands, as discussed in Section 3.4. Section shear failure can also occur when compressive struts develop due to arch action within a member and initiate concrete failure in compression, which then also rapidly degrades the shear capacity of the section. Thus, the failure criteria used to establish structural failure of the PCCV in the global modeling are 1) the strain level in rebars causing rupture of the bar, 2) the level of shear strain across a structural section that indicates the shear capacity is exceeded, and 3) the strain level causing rupture of prestressing tendons.

As the limit state for section shear failure, a criteria for concrete shear strain across a section is defined. This failure criterion has been established for the modeling methodology employed based on previous work and benchmarking with experimental tests on structural specimens, References 5.3.12, 5.3.13, and 5.3.14. Once a shear band forms and the concrete shear strains reach a median level of .55% across the complete section, a brittle type shear failure of the section will occur. This criteria is needed, independent of rebar performance, because this structural failure mode can develop before rebar rupture or even rebar yield is reached in the analysis. The median and 95% confidence values for this concrete section shear strain are shown in Table 3-10. Note that this failure criteria is considered independent of temperature, but because the concrete properties degrade with temperature, the section shear capacity is reduced with temperature.

The rupture strain for Grade 60 reinforcing bars is based on the elongation limits from test data. The test specimen elongation strain is then factored to account for strain concentration factors that are not captured by the finite element modeling, which is based on smeared cracking. In reinforced concrete structures, cracking generally develops in a series of discrete cracks, and the strain in the rebar is intensified at the intersection of these discrete cracks. From previous experience with similar modeling (References 5.3.10, 5.3.11 and 5.3.12), this strain concentration factor has a median value of 2.0, and the calculated strain at which rebar rupture can occur is generally taken to be 5% at room temperature. The median and 95% confidence values as a function of temperature for rebar fracture strain are summarized in Table 3-10.

For greased prestressing tendons, there is no strain concentration factor introduced due to cracking because the tendon acts independent of the concrete strain along the direction of the tendon. Thus, the rupture strain is based on nominal reductions in the elongation data for the tendons strands. The median and 95% confidence values as a function of temperature for tendon rupture strain are summarized in Table 3-10.

Failure criteria are also defined to consider leakage due to tearing of the liner. Tests of over-pressurization of PCCV scale models show that liner tearing will develop at discontinuities where strain concentration factors exist, in particular at the connections of liners with thicker plates at penetrations or geometric discontinuities. From previous work, for example Reference 5.3.15, this failure criterion for a tearing strain is based on the ductility of the material and the magnitude of strain concentration factors not captured by the fidelity of the modeling. First, the ductility of the liner material is defined based on elongation data performed on uniaxial test specimens. The ductility depends on the state of stress, which is generally biaxial or triaxial loading. For the liner at penetrations, the loading due to internal pressure is biaxial with the hoop tension twice that of the tension in the axial direction. This biaxial loading produces a ductility limit of 60% of the uniaxial elongation data. In addition, to account for reduced ductility in the heat affected zones of welds in the liner, a further reduction of 15% on the uniaxial test data is used. This ductility limit must then be further reduced for comparison to calculated liner strains to account for the strain concentration factors not captured in the analyses. This factor depends on the fidelity of the modeling. In the global model, the liner strains are taken at the local areas showing distress, that is, local strains rather than far field strains, and a median strain concentration factor of 6 is used on the ductility limit to establish liner tearing. For the thicker steel components of the penetration, the loading can be triaxial, and the elongation data is factored by 50% to determine the material ductility. The median and 95% confidence values for these failure criteria are summarized in Table 3-10. These values are consistent with those used in similar previous work described in Reference 5.3.10.

**Table 3-10**  
**Summary of Material Limits and Failure Criteria**

Criteria	Normal Operating Conditions (150 °F)		Long Term Accident Conditions (500 °F)		Hydrogen Burning Conditions (1000 °F)	
	Median	95 %	Median	95 %	Median	95 %
Section Shear Strain (%)	.55	.44	.55	.44	.55	.44
Rebar Fracture Strain (%)	5.0	2.0	5.5	2.2	6.0	2.4
Tendon Failure Strain (%)	2.66	2.50	2.80	2.60	3.00	2.74
Liner Tearing Strain (%) (1/4" Thick, Grade 60)	2.13	1.72	2.16	1.45	3.54	2.42
Liner Tearing Strain (%) (>1/4" thick, Grade 70)	1.72	1.40	1.75	1.17	2.87	1.96

## **4.0 PRESTRESSED CONCRETE CONTAINMENT**

### **4.1 Model Description**

A global 3D model is used to assess the ultimate capacity of the PCCV due to over-pressurization under severe accident conditions. This global modeling is needed to capture the overall structural performance and potential failure modes of the primary containment system and is sufficiently accurate to determine the ultimate pressure capacity of the PCCV components, governed by concrete, tendon, and rebar strength and their interaction. The ultimate capacity for the PCCV is based on strain limits for rebar and tendon rupture, concrete compressive stress, or concrete shear strain limits that indicate section shear failure. The concrete constitutive model includes tensile cracking, shear shedding, and compressive crushing as material limits. As loads are redistributed due to these material limits, the increasing loads will eventually lead to section failures. Also, an evaluation of liner tearing can be determined from the global model by considering calculated liner strains at distressed locations and factoring for strain concentration factors, based on previous similar analyses, to account for discontinuities at anchorages and connections. This evaluation for liner tearing also considers reduced ductility of the liner material due to biaxial loading conditions and for heat affected zones at weld seams.

The modeling consists of a free-standing, full height representation of the PCCV. The thermal model, illustrated in Figure 4-1, is used to determine the temperature distribution within the structure for each of the 3 thermal conditions, and the stress model, illustrated in Figure 4-2, is used to determine the pressure capacity based on the temperature distribution of interest and the combinations of the other parameter values. Steady state temperature solutions are used for the normal operating and long term accident cases. A transient thermal solution is used for the hydrogen burning case with the initial conditions set to the steady state operating conditions. The appropriate temperature distribution is then transferred to the stress model, and the internal pressure is incrementally increased to find the failure pressure with that temperature distribution.

As illustrated in the figures, the concrete is modeled with solid elements and the steel liner is modeled with plate elements. The liner elements are attached to the common nodes on the surfaces of the concrete elements for compatibility with the concrete deformations. This assumes that the liner anchorage system keeps the liners in contact with the concrete for this global modeling of the PCCV performance. The prestressing tendons are modeled with truss elements using independent nodes from the concrete nodes. The tendon nodes are then constrained to the concrete nodes using constraint equations to capture the behavior of the greased tendons. For the hoop tendons, the tendons are constrained to the concrete in the radial and axial directions, but the tendon nodes are allowed to move relative to the concrete in the hoop direction. Similarly, for the axial tendons, the tendons are constrained to the concrete in the radial and hoop directions but are allowed to move relative to the concrete in the axial direction. For the areas with significant tendon curvature, for example the axial tendons in the dome and the tendons that wrap around the penetrations, the tendon nodes are fully constrained to the concrete. This tendon modeling is illustrated in Figure 4-3. The prestress loads are applied using an initial stress in the tendon elements. The tendon elements are divided into groups to allow variation in the initial stress distribution to simulate prestressing losses.

The reinforcement bars are modeled as embedded, truss-like steel elements at the appropriate locations within the concrete brick elements. The strains within the brick element at the locations of the rebar within that element are used to assess the rebar performance via the constitutive relations for the steel material. The associated stiffness and stress in the reinforcement are superimposed onto the concrete brick element. The reinforcement included in the modeling is illustrated in Figures 4-4 through 4-8, showing axial bars on the inner surface, axial bars on the outer surface, hoop bars on the inner surface, hoop bars on the outer surface, and other secondary reinforcement, respectively. As illustrated, some smearing of the reinforcement is performed to reduce modeling and computation times, for example, every other bar may be explicitly included but each with twice the area (2:1 modeling). In some areas, 4 bars are lumped together as a single truss-like sub-element with 4 times the individual rebar area (4:1).



**Figure 4-1 Full 3D Finite Element Modeling for Thermal Analysis**



**Figure 4-2 Full 3D Finite Element Modeling for Stress Analysis**

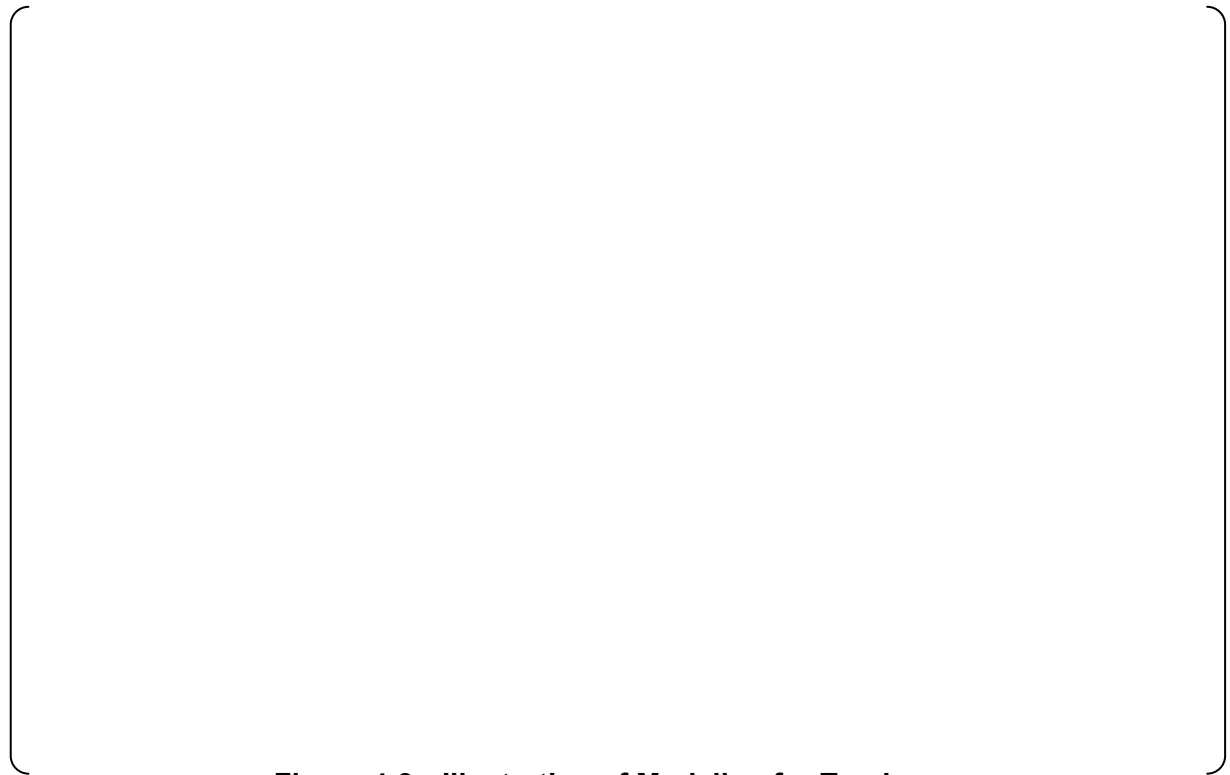


**Figure 4-3 Illustration of Modeling for Tendons**

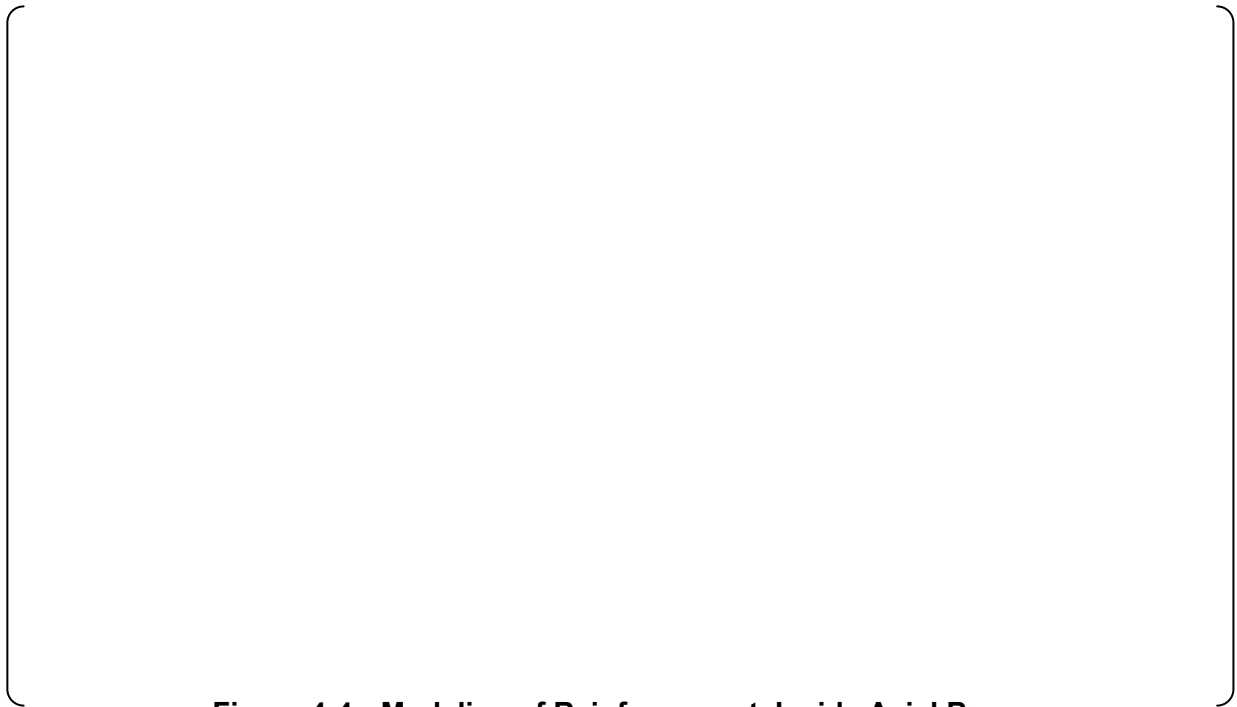


**Figure 4-4 Modeling of Reinforcement, Inside Axial Bars**



**Figure 4-5 Modeling of Reinforcement, Outside Axial Bars**



**Figure 4-6 Modeling of Reinforcement, Inside Hoop Bars**



**Figure 4-7 Modeling of Reinforcement, Outside Hoop Bars**



**Figure 4-8 Modeling of Reinforcement, Other Bars**

#### **4.2 Thermal Analyses**

The thermal model is used to develop the temperature distributions for the stress model in performing the pressure capacity analyses. The temperature distributions determine the variation of material properties with temperature within the structure and thermal stresses based on the changes from reference temperature and restraint against thermal expansion or contraction. The 3 thermal conditions described in Section 3.6 are used as the basis for evaluating the variation of pressure capacity with temperature. The temperature distributions associated with these 3 thermal conditions are illustrated in Figure 4-9 for normal operating condition, Figure 4-10 for long term accident condition, and Figure 4-11 for the hydrogen burning thermal condition. The temperature distribution for the normal operating condition is based on a steady state solution with the PCCV atmosphere at 105 °F. The temperature distribution for the long term accident thermal condition is based on a steady state solution with the PCCV atmosphere at 438 °F. The temperature distribution for the hydrogen burning thermal condition is based on a transient solution when the PCCV atmosphere and liner reach 1000 °F for a postulated hydrogen burn scenario. All 3 thermal conditions are considered to occur during extreme winter ambient conditions when the air temperature is -40 °F. The temperature gradient through the PCCV wall for the transient hydrogen burning case is illustrated in Figure 4-11. For the steady state based conditions, the gradient is linear through the wall.



**Figure 4-9 Temperature Distribution for Normal Operating Condition**



**Figure 4-10 Temperature Distribution for Long Term Accident Condition**

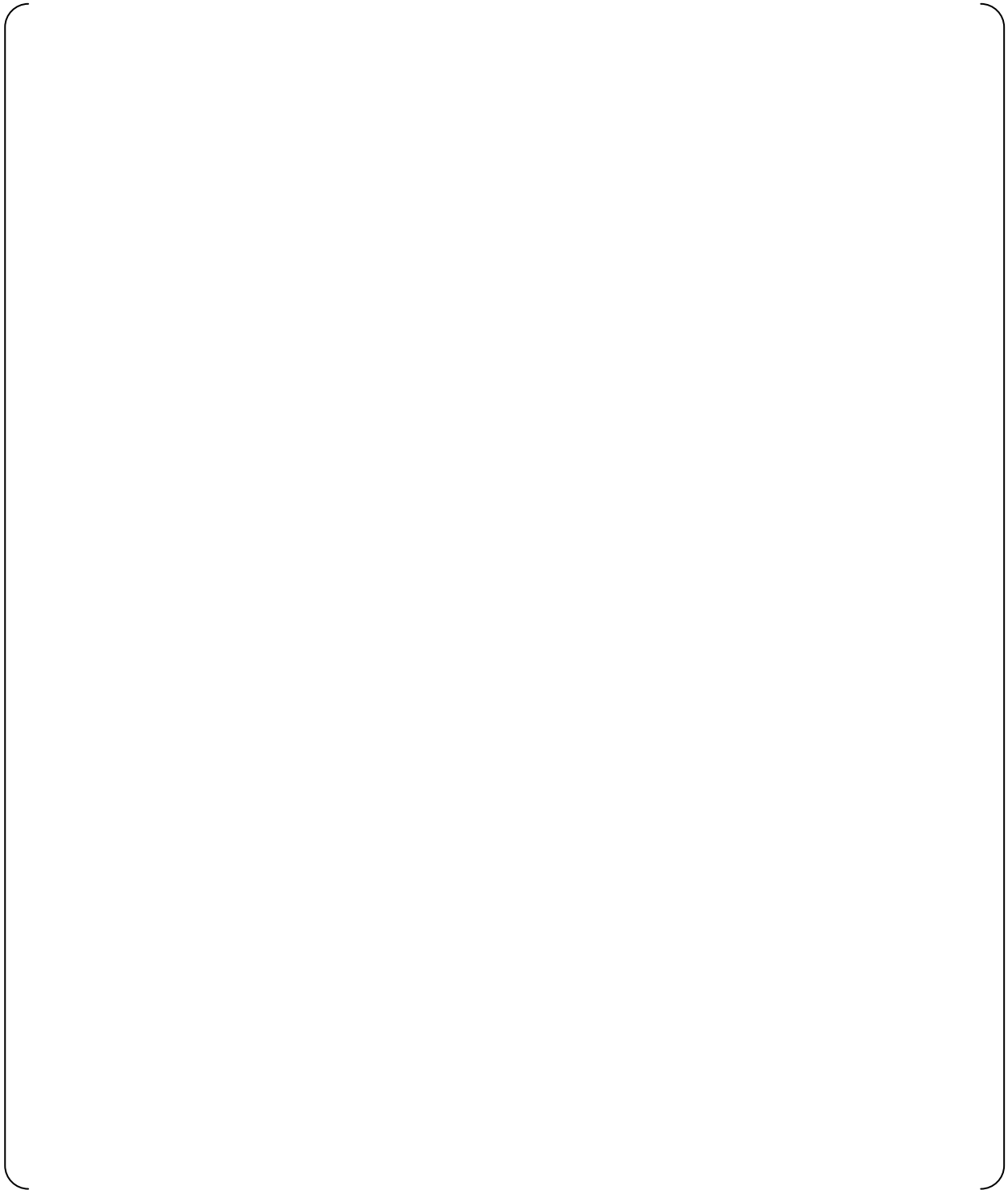


**Figure 4-11 Temperature Distribution for Hydrogen Burning Condition**

### 4.3 Median Capacity Analyses

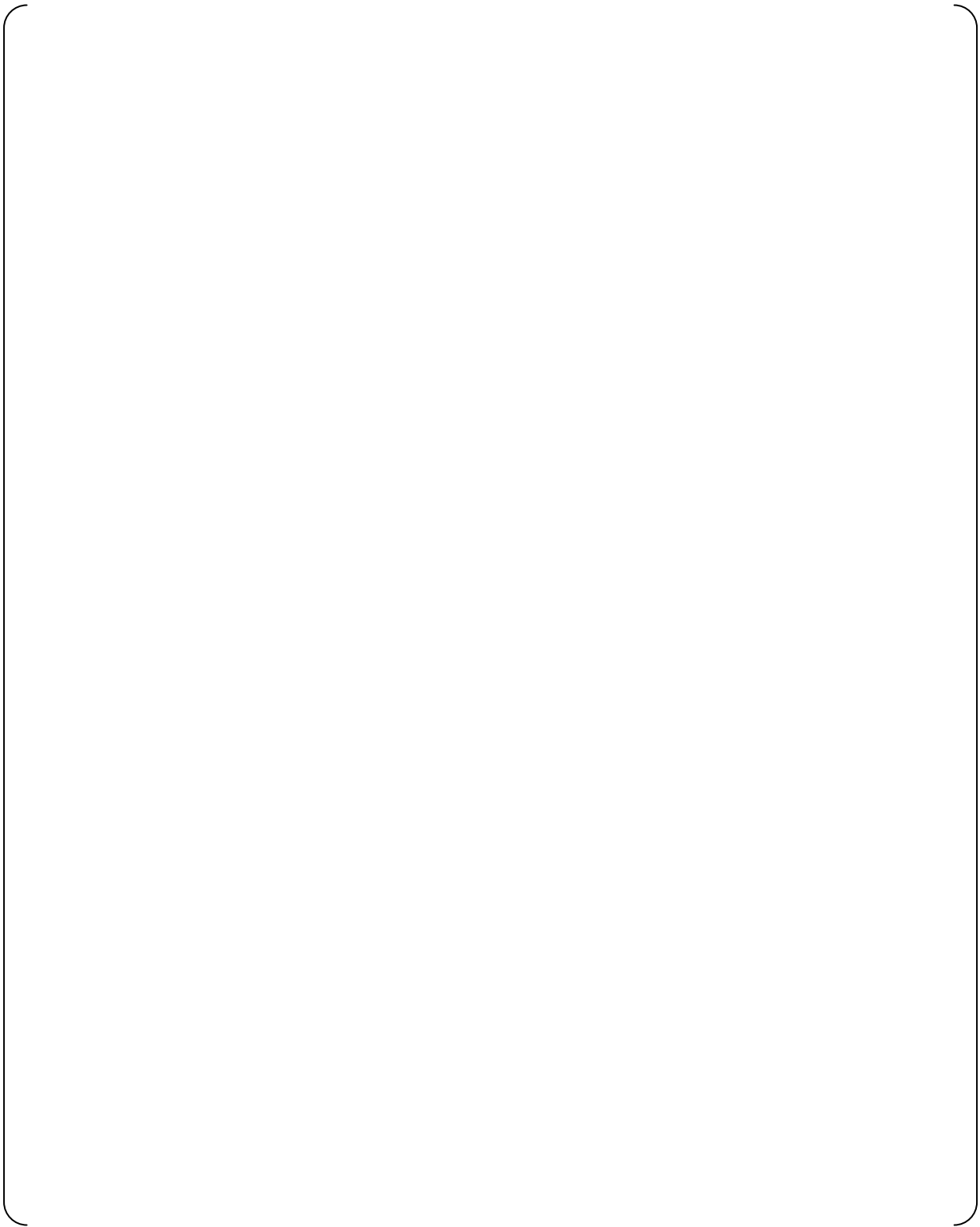
The median ultimate pressure capacity for the PCCV is determined using the global stress model along with median values of all material properties and failure criteria. The median pressure capacity is performed for each of the 3 thermal conditions described in Section 3.6 and illustrated in the previous section. For each median pressure capacity analysis, the failure pressure for each mode of failure is determined based on the corresponding failure criteria. For example, monitoring liner plastic strains to determine the pressure where liner tearing initiates. The failure pressures for each failure mode are determined independently, that is, the structural effect or consequences due to initiation of any one failure mode does not influence the next failure mode. For example, when the rupture strain of a rebar has been reached, the pressure associated with rebar failure is determined, but the rebar continues to plastically deform until the next failure mode is reached. This complies with the basic assumptions needed for parameter independence in the probabilistic assessment.

Table 4-1 summarizes the median pressure capacities calculated for the various failure modes for the 3 thermal conditions. The following figures illustrate the performance of the PCCV during over-pressurization for the steady state long term accident thermal condition. Figure 4-12 provides a contour plot for accumulated plastic strain in the liner illustrating the failure mode for liner tearing. The contour limit has been set to the failure strain at the corresponding temperature so that red color indicates areas near the failure limit. In this plot the peak plastic strain is shown to be above the failure limit so that liner tearing has initiated. Figure 4-13 provides a contour plot for maximum principal strains in the concrete. In this figure, the contour limit is set to 2% to highlight the areas of more extensive cracking to illustrate the cracking damage that develops leading to yield and rupture of rebar and tendons. Figure 4-14 provides a contour plot for plastic strain in the hoop tendons illustrating failure mode associated with tendon rupture. In this plot, the peak plastic strain is still below the failure strain limit, so that tendon failure has not yet developed. It is noted that the deformed shape and failure mode associated with rebar and tendon rupture illustrated in these figures closely matches that in the ¼ scale PCCV tests conducted at Sandia (References 5.3.17 and 5.3.18).

Figures 4-15, 4-16, and 4-17 provide similar plots for the analyses to calculate the median pressure capacity at the normal operating condition. Figures 4-18 4-19, and 4-20 provide similar plots for the median pressure analyses for the hydrogen burning condition.

**Table 4-1 Summary of Median Pressure Capacities**

Failure Mode	Failure Pressure (psig)		
	Normal Operating Conditions	Long Term Accident Conditions	Hydrogen Burning Conditions
PCCV Liner Tearing	230.0	223.6	238.5
PCCV Rebar Rupture	250.0	243.6	244.5
PCCV Tendon Rupture	248.0	243.6	249.0
PCCV Concrete	252.0	255.6	255.7



**Figure 4-12 Accumulated Plastic Strain in Liner, Median Pressure Capacity for Long Term Accident Condition**

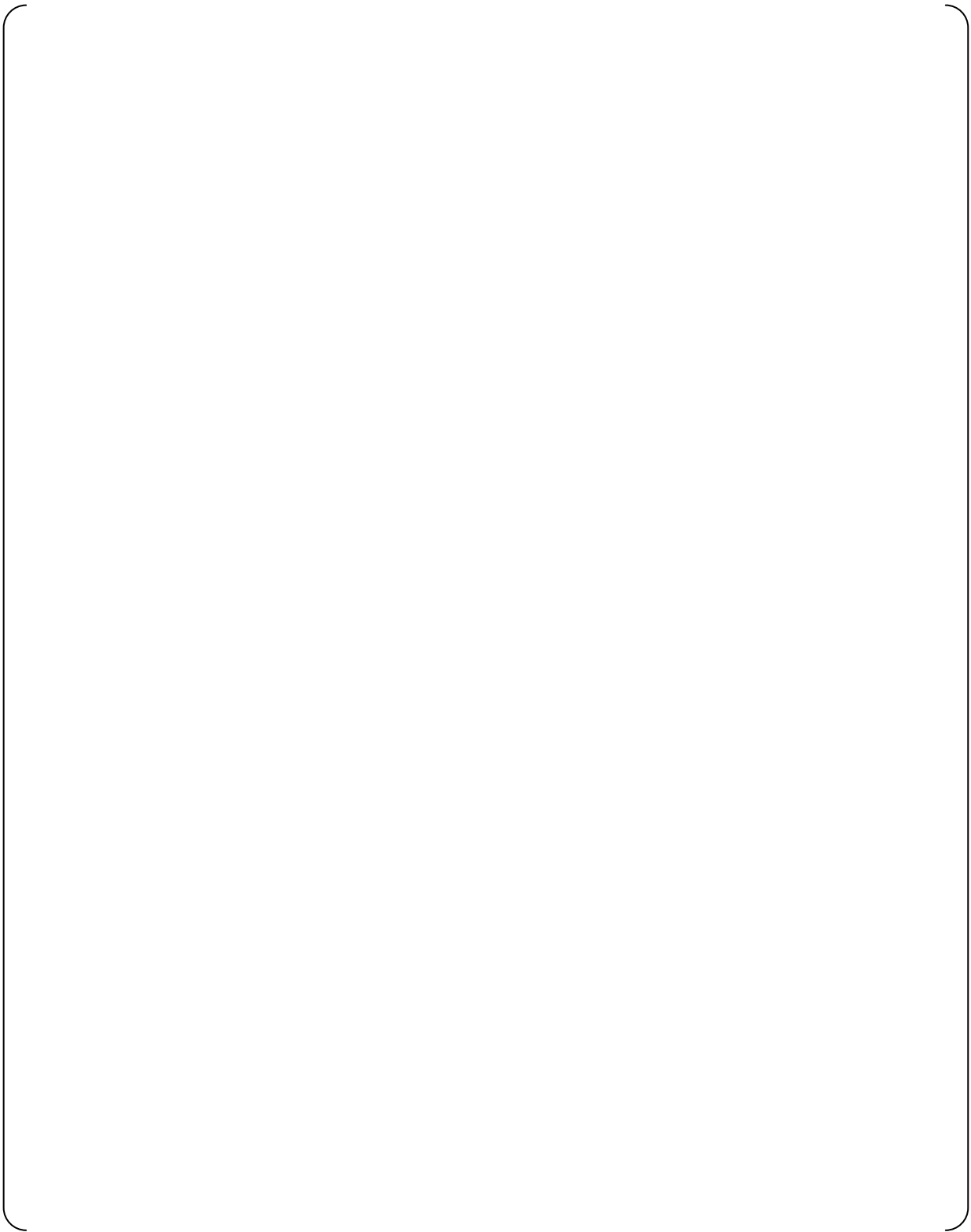


**Figure 4-13 Maximum Principal Concrete Strains, Median Pressure Capacity for Long Term Accident Condition**



**Figure 4-14 Accumulated Plastic Strain in Hoop Tendons, Median Pressure Capacity for Long Term Accident Condition**

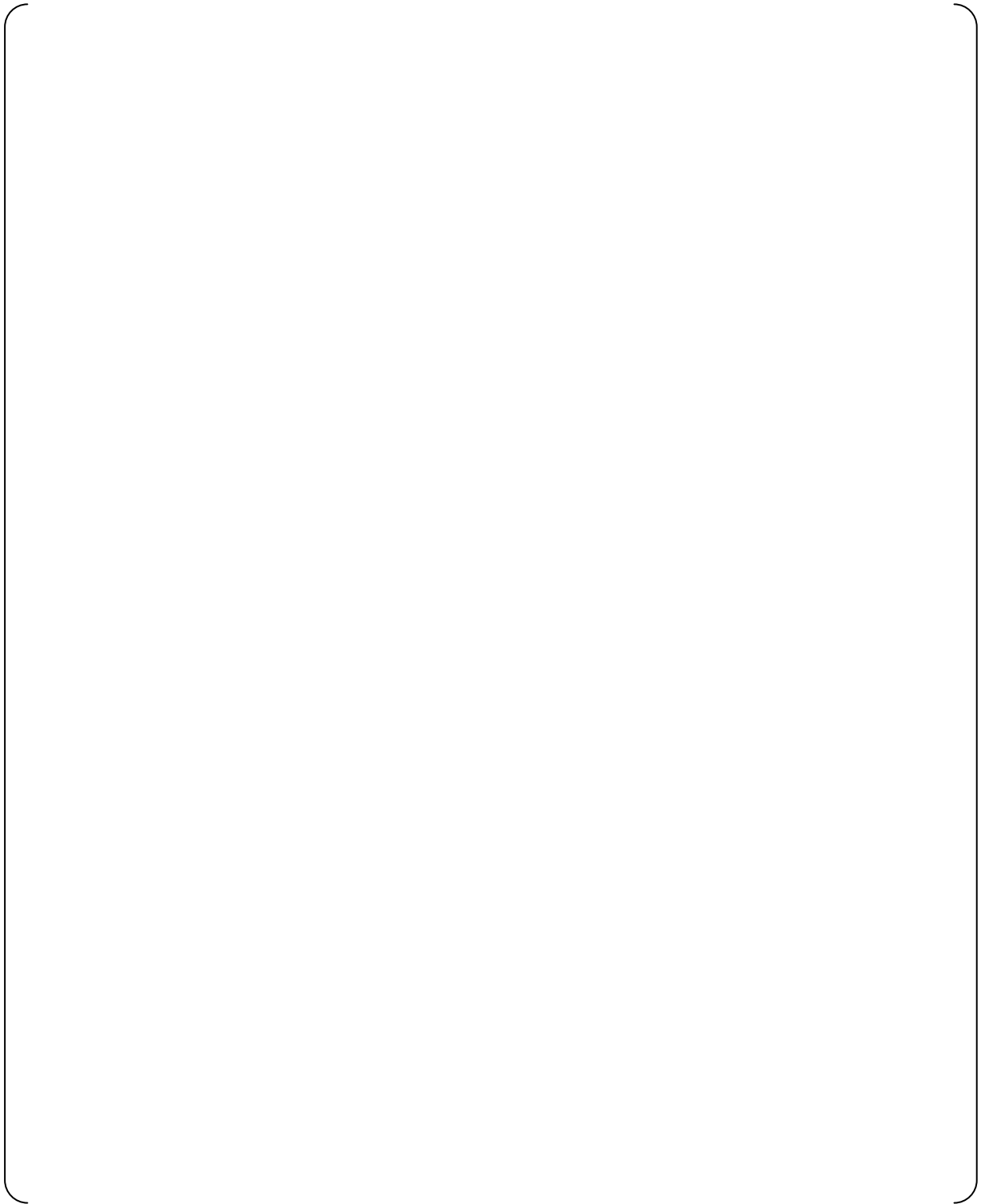


**Figure 4-15 Accumulated Plastic Strain in Liner, Median Pressure Capacity for Normal Operating Condition**

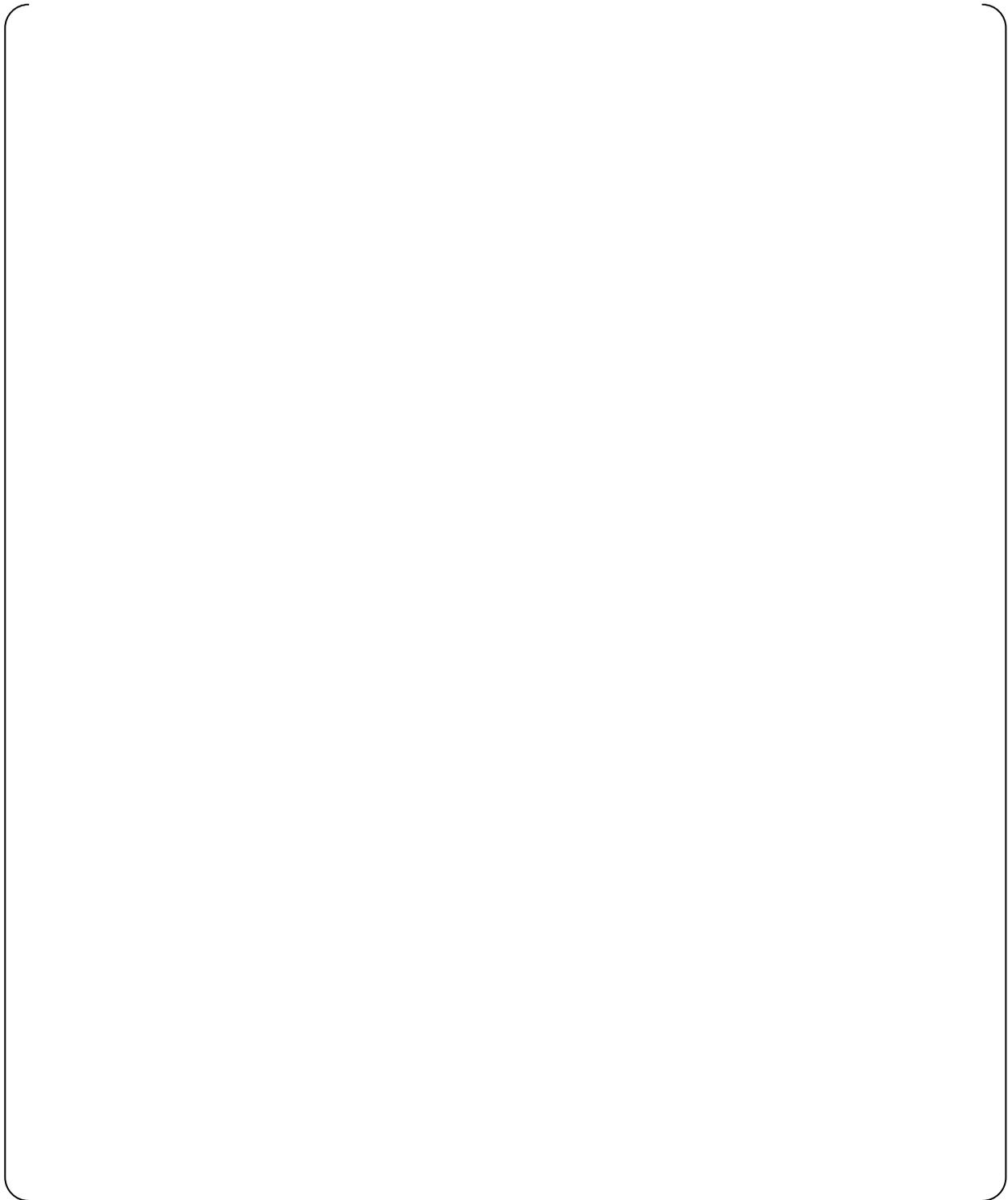


**Figure 4-16 Maximum Principal Concrete Strains, Median Pressure Capacity for Normal Operating Condition**



**Figure 4-17 Accumulated Plastic Strain in Hoop Tendons, Median Pressure Capacity for Normal Operating Condition**

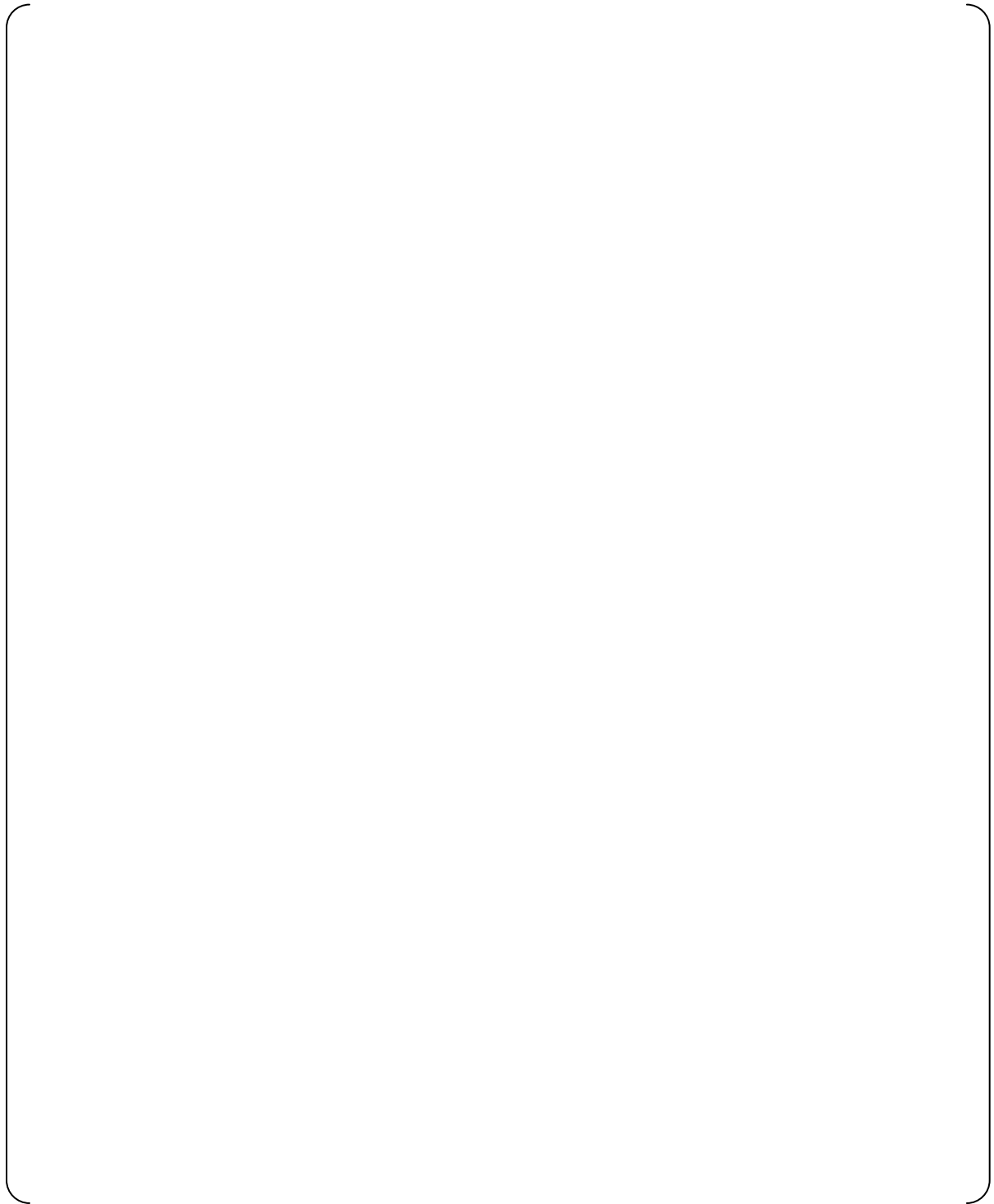


**Figure 4-18 Accumulated Plastic Strain in Liner, Median Pressure Capacity for Hydrogen Burning Condition**

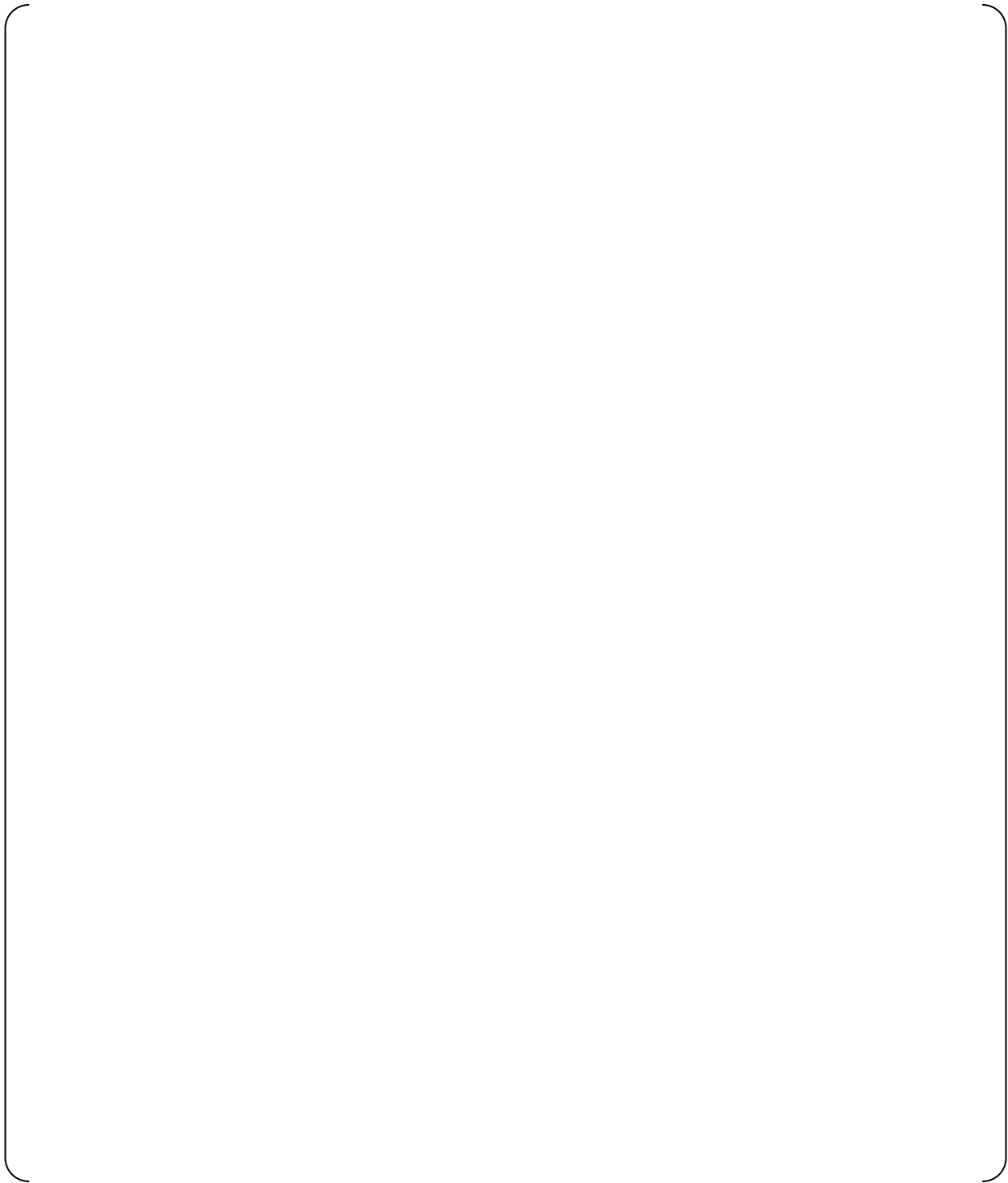


**Figure 4-19 Maximum Principal Concrete Strains, Median Pressure Capacity for Hydrogen Burning Condition**



**Figure 4-20 Accumulated Plastic Strain in Hoop Tendons, Median Pressure Capacity for Hydrogen Burning Condition**

#### 4.4 Evaluation for Uncertainty

The evaluation of uncertainty to determine the variance in the pressure capacity is performed with the global stress model using the temperature distribution for the long term accident condition. It is assumed that the uncertainty does not change significantly for the other temperature conditions, just the median pressure capacity. Analyses are performed using variations for each parameter determined to have a significant effect on the pressure capacity as described in Sections 3.3 and 3.4. For example, for each significant material property, the 95% confidence value of the property is used along with the median values of all other properties to determine the effect on the calculated pressure capacity for that property. Similarly, for each failure criteria, the 95% confidence value for that failure criterion is used to determine the pressure capacity using the median values for all material properties. Table 4-2 summarizes the variations performed and the corresponding pressure capacities for each failure mode. Using the procedure described in Section 3.3, the variance or deviation is calculated for each parameter. For example the variance in the calculated pressure capacity for liner tearing due to uncertainty in rebar yield is calculated as

$$\beta_s^{rebar-yield} = \frac{\text{Ln}(217.6 / 223.6)}{-1.645} = .0165$$

The variance for each parameter variation is combined together along with the modeling variance using the Square Root of the Sum of the Squares to define a composite variance on the pressure capacity for that failure mode.

**Table 4-2 Summary of Uncertainty Evaluations in Global Modeling**

Variation Considered (Using Long Term Accident Conditions)	Failure Pressure (psig)			
	Liner Tearing	Rebar Rupture	Tendon Rupture	Concrete Failure
Median Values	223.6	243.6	243.6	255.6
Concrete Strength and Stiffness	222.8	243.0	243.0	251.0
Concrete Temperature Effect	221.6	241.6	241.6	253.0
Rebar Yield & Ultimate Strength	217.6	241.0	239.6	250.0
Tendon Prestressing Level	223.0	243.6	243.6	255.6
Tendon Yield and Ultimate Strength	215.6	237.6	241.6	
Rebar Rupture Strain		217.6		
Tendon Rupture Strain			241.6	
Liner Rupture Strain	217.0			
Concrete Failure Strain				254.0

#### 4.5 Fragility Summary

The global modeling is used to establish the ultimate capacity and pressure fragility of the PCCV boundary for the primary containment system. The steady state thermal condition representative of long term accidents is used as a basis for evaluation of aleatory uncertainties in material properties and failure criteria. The variation of the fragility with temperature is evaluated through consideration of a range in thermal conditions. The failure pressure is characterized using a lognormal probability density function defined as

$$p_f(p) = \frac{1}{p\beta\sqrt{2\pi}} \exp\left[-\frac{1}{2}\left(\frac{\ln(p) - \mu}{\beta}\right)^2\right]$$

where  $p$  is the failure pressure,  $\mu$  is the mean value of the natural log of the failure pressure, and  $\beta$  is the standard deviation of the natural log of the failure pressure. The corresponding fragility, defined as the cumulative probability of failure for increasing internal pressure is defined with the integral of the probability density function. The failure pressures are summarized in Table 4-3, which provides the median and 95% confidence values of the failure pressures for the various failure modes and temperature regimes. The 95% confidence value is the pressure value such that there is a 95% confidence that the actual failure pressure will be higher. The pressure fragility with temperature are plotted in Figures 4-21, 4-22, 4-23, and 4-24, for liner tearing, rebar failure, tendon failure, and concrete failure, respectively.

**Table 4-3**  
**Summary of Pressure Fragility from Global Modeling**

Failure Mode and Thermal Condition	Failure Pressure (psig)	
	Median	95% HC
PCCV Liner Tearing		
Normal Operating	230.0	184.9
Long Term Accident	223.6	176.0
Hydrogen Burning	238.5	183.7
PCCV Rebar Rupture		
Normal Operating	250.0	195.9
Long Term Accident	243.6	187.2
Hydrogen Burning	244.5	184.2
PCCV Tendon Rupture		
Normal Operating	248.0	200.7
Long Term Accident	243.6	192.9
Hydrogen Burning	249.0	192.9
PCCV Concrete Failure		
Normal Operating	252.0	203.7
Long Term Accident	255.6	202.2
Hydrogen Burning	255.7	197.9

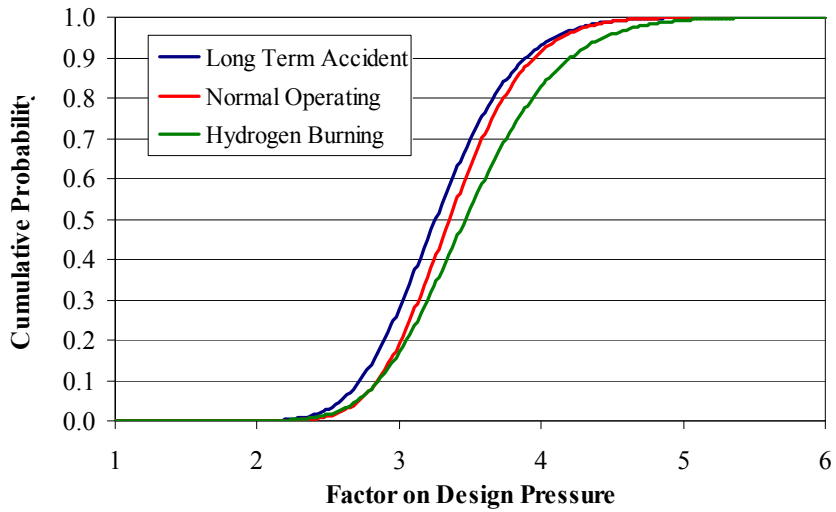


Figure 4-21 Pressure Fragility with Temperature for PCCV Liner Tearing

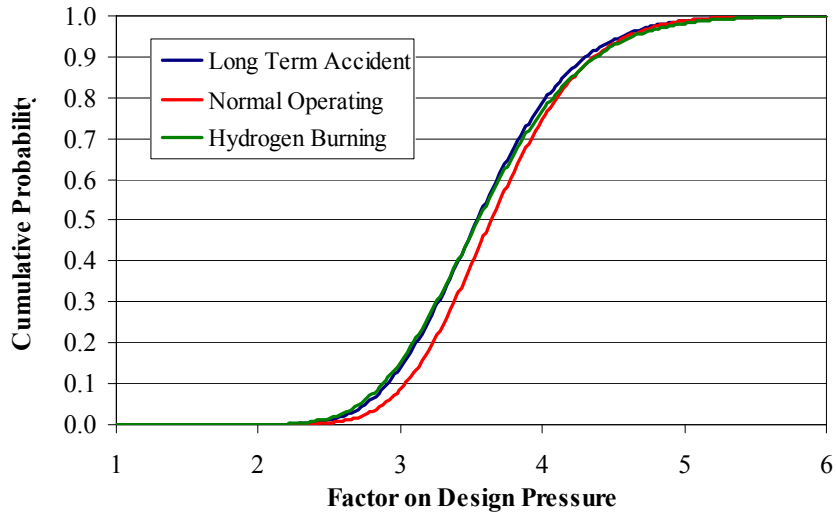


Figure 4-22 Pressure Fragility with Temperature for PCCV Rebar Failure

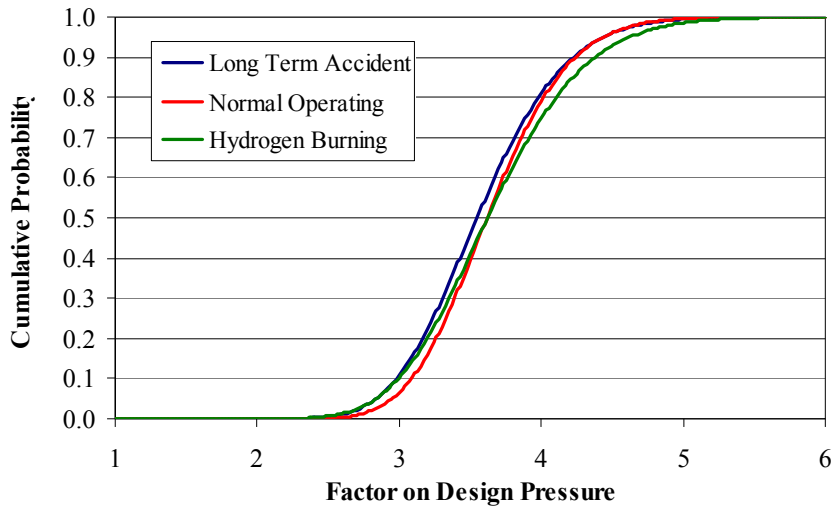


Figure 4-23 Pressure Fragility with Temperature for PCCV Tendon Failure

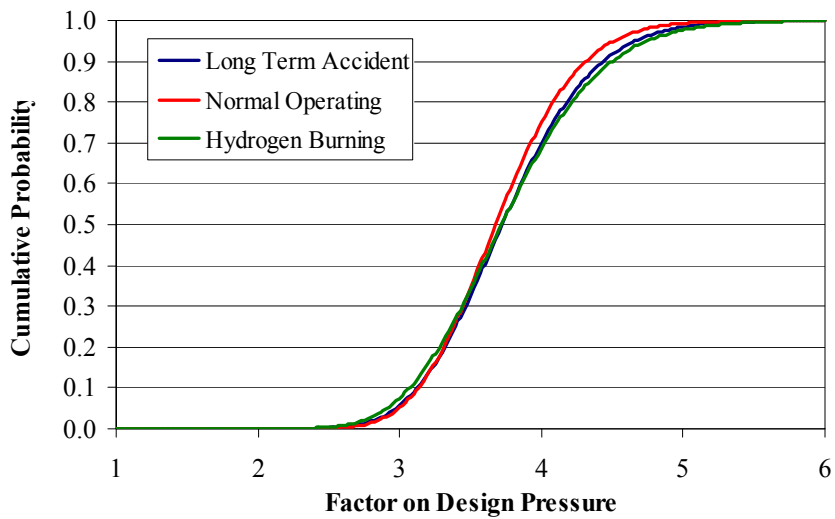


Figure 4-24 Pressure Fragility with Temperature for PCCV Concrete Failure

## **5.0 APPLICABLE DOCUMENTS**

### **5.1 Project Documents**

- 5.1.1. Design Control Document for US-APWR, Chapter 3, Design of Structures, Systems, Components and Equipment, MUAP DC003, Revision 2, October 2009.
- 5.1.2. US-APWR Probabilistic Risk Assessment, MUAP-07030-P Rev. 2 (Proprietary), December 2009

### **5.2 Codes and Standards**

- 5.2.1. ASME 2004: Boiler and Pressure Vessel Code, Section III – Rules for Construction of Nuclear Power Plant Components, Division 2 – Code for Concrete Reactor Vessels and Containments, Subsection CC- Concrete Containments, Article CC 3000 – Design.
- 5.2.2. ASME 2004: Boiler and Pressure Vessel Code, Section II, Part A – Ferrous Material Specifications.
- 5.2.3. ACI-349-01, Code Requirements for Nuclear Safety Related Concrete Structures.
- 5.2.4. ASME 2004: Boiler and Pressure Vessel Code, Section III – Rules for Construction of Nuclear Power Plant Components, Division 1 – Subsection NE – Class MC Components.

### **5.3 Reference Documents**

- 5.3.1. ABAQUS/Standard, Version 6.9, Dassault Systemes Simulia Corp., Providence, RI.
- 5.3.2. ANACAP-U, Version 2.5, Theory Manual, ANA-QA-145, ANATECH Corp., San Diego, CA, 1998.
- 5.3.3. Rodabaugh, E. C., and Desai, K. D., “Realistic Seismic Design Margins of Pumps, Valves, and Piping,” NUREG/CR-2137, USNRC, Washington, DC, June 1981.
- 5.3.4. Chu, T. Y., Pilch, M. M., et. al., “Lower Head Failure Experiments and Analyses,” NUREG/CR-5582, USNRC, Washington, DC, February 1999.
- 5.3.5. Brister, P. M., “Code Design Criteria in the USA, Evaluation of Strength Properties,” Proceedings of the 3<sup>rd</sup> International Conference on Pressure Vessel Technology, Tokyo, Japan, April 18-22, 1977.
- 5.3.6. Luecke, W. E., et. al., “Mechanical Properties of Structural Steels,” NIST NCSTARR 1-3D, Federal Building and Fire Safety Investigation of the World Trade Center Disaster, National Institute of Standards and Technology, Washington, DC, September 2005.
- 5.3.7. Bournonville, M., Dahnke, J., and Darwin, D., “Statistical Analysis of the Mechanical Properties and Weight of Reinforcing Bars,” Report SL 04-1, Structural Engineering and Engineering Mechanics, University of Kansas, December 2004.
- 5.3.8. Specification Sheets for PC Strand to ASTM A416, Sumiden Wire Products Corporation (SWPC), Stockton, CA.
- 5.3.9. Freskakis, G. H., “State-of-the-Art Report on High Temperature Concrete Design,” Burns and Roe, Inc., Oradell, NJ, for U. S. Department of Energy, DOE/CH/94000-1, November 1985.

- 5.3.10. James, R. J., Rashid, Y. R., Liu, A. S., and Gou, B., "*Fragility Analysis for the Pressure Capacity of ESBWR Primary Containment System*," Proceedings of the 2007 International Congress on Advances in Nuclear Power Plants, ICAPP07, Nice, France, May 13-18, 2007.
- 5.3.11. James, R. J., Zhang, L., Rashid, Y. R., "Impact of High Velocity Objects into Concrete Structures – Methodology and Application," Proceedings of ASME International Mechanical Engineering Congress and Exposition, Washington, D. C., November, 2003.
- 5.3.12. James, R. J. and Rashid, Y. R., "Severe Impact Dynamics of Reinforced Concrete Structures," Sixth European Conference on Structural Dynamics, Paris, France, September, 2005.
- 5.3.13. James, R. J., Zhang, L., Rashid, Y. R., Cherry, J. L., "Seismic Analysis of a Prestressed Concrete Containment Vessel Model," NUREG/CR-6639, U. S. Nuclear Regulatory Commission, Washington, D. C., August 1999.
- 5.3.14. James, R. J., Zhang, L., Rashid, Y. R., Cherry, J. L., "Seismic Analysis of a Reinforced Concrete Containment Vessel," NUREG/CR-6707, U. S. Nuclear Regulatory Commission, Washington, D. C., August 1999.
- 5.3.15. Dameron, R. A., Dunham, R. S., Rashid, Y. R., Sullaway, M. F., "Criteria and Guidelines for Predicting Concrete Containment Leakage," Fourth Workshop on Containment Integrity, Sponsored by USNRC, Arlington, VA, June 1988.
- 5.3.16. Pfeiffer, P. A., Kennedy, J. M., and Marchertas, A. H., "Thermal Effects in Concrete Containment Analysis," NUREG/CP-0095, and Fourth Workshop on Containment Integrity, Sponsored by USNRC, Arlington, VA, June 1988.
- 5.3.17. Dameron, R. A., Zhang, L., Rashid, Y. R., Vargas, M. S., "Pretest Analysis of a 1:4-Scale Prestressed Concrete Containment Vessel Model," NUREG/CR-6685, U. S. Nuclear Regulatory Commission, Washington, D. C., October 2000.
- 5.3.18. Dameron, R. A., Hansen, B. E., Parker, D. R., Rashid, Y. R., "Posttest Analysis of the NUPEC/NRC 1:4-Scale Prestressed Concrete Containment Vessel Model," NUREG/CR-6809, U. S. Nuclear Regulatory Commission, Washington, D. C., February 2003.
- 5.3.19. Ang, A. H-S. and Tang, W. H., *Probability Concepts in Engineering, Emphasis on Applications to Civil and Environmental Engineering*, John Wiley & Sons Inc., New Jersey, 2007.
- 5.3.20. Draft Regulatory Guide, DG-1203 "Containment Performance for Pressure Loads", U. S. Nuclear Regulatory Commission, December 2008.
- 5.3.21. "Nonlinear, Incremental Structural Analysis of Massive Concrete Structures", ETL 1110-2-365, U. S. Army Corps of Engineers, Department of the Army, Washington, DC, August 1994.